Mineral Petrol (2008)
DOI 10.1007/s00710-007-0222-4
Printed in The Netherlands

Mineralogy and Petrology

Pre-metamorphic melt infiltration in metasediments: geochemical, isotopic (Sr, Nd, and Pb), and field evidence from Serie dei Laghi (Southern Alps, Italy)

L. Pinarelli[1], **M. A. Bergomi**[2], **A. Boriani**[3], **E. Giobbi**[2]

[1] CNR – Istituto di Geoscienze e Georisorse, Sezione di Firenze, Firenze, Italy
[2] Dipartimento di Scienze Geologiche e Geotecnologie, Università Milano-Bicocca, Milano, Italy
[3] Dipartimento di Scienze della Terra, Università degli Studi di Milano, Milano, Italy

Received February 20 2007; Accepted October 10 2007; Published online May 5 2008

Editorial handling: B. deVivo

Summary

Gradual transitions from K-feldspar free gneisses to K-feldspar bearing augengneisses are sometimes observed in metamorphic terranes. They have been explained with metasomatic porphyroblastic growth connected with regional metamorphism, or with pre-metamorphic presence of magmatic megacrysts. A transition of this kind can be observed in the Serie dei Laghi (Southern Alps, Italy), where coarse-grained metarenites (*Cenerigneiss*) grade into *Ceneri augengneisses* with large K-feldspar porphyroclasts, and *banded amphibolites* of the ''Strona Ceneri Border Zone'' grade into *Hbl augengneisses* rich in K-feldspar.

The *Ceneri augengneisses* are chemically indistinguishable from the *Cenerigneiss*, but have higher $^{87}Sr/^{86}Sr$ (0.7256–0.7258 vs. 0.7215–0.7233), similar to those of the Ordovician granites that were intruded, before the regional metamorphism, into the protoliths of both *Cenerigneiss* and *amphibolites*. The *Cenerigneiss* contains two types of zircons: (1) highly luminescent, rounded grains or fragments, yielding U–Pb SHRIMP ages from 0.43 to 1.0 Ga; (2) euhedral grains with oscillatory zoning (magmatic), with U–Pb SHRIMP concordant ages of 466 ± 13 Ma. This age coincides with the Rb–Sr whole rock emplacement age of the Ordovician granitoids (466 ± 5 Ma).

Correspondence: L. Pinarelli, CNR – Istituto di Geoscienze e Georisorse, Sezione di Firenze, Via La Pira 4, 50121 Firenze, Italy
e-mail: lapina@igg.cnr.it

The *Hbl augengneisses* form three groups with distinct geochemical patterns, whose distributions on inter-element diagrams trend towards the Ordovician meta-granites and meta-aplites. In addition, the *Hbl augengneisses* have higher $^{87}Sr/^{86}Sr$ (0.7132–0.7147 vs. 0.7031–0.7046) and lower $^{143}Nd/^{144}Nd$ (0.51214–0.51219 vs. 0.51273–0.51297) than the *amphibolites*, suggesting the addition of an isotopically evolved component.

The observed chemical and isotope patterns, as well as the vicinity of the augen gneisses to the Ordovician intrusions, lead us to conclude that the *Ceneri augengneisses* and *Hbl augengneisses* are the result of infiltration of residual hydrous magmas into the protolith of both the Cenerigneiss and the amphibolites at the time of Ordovician granite emplacement, long before the regional metamorphism in the Serie dei Laghi.

Introduction

The gradual appearance of K-feldspar megacrysts in deformed gneisses is quite a common feature in metamorphic areas. A porphyroblastic origin is generally taken to imply metasomatism during regional metamorphism. This is discussed, for example, by Kano (1991) who interpreted the augen gneiss of the Katakai area as the result of metasomatic growth of K-feldspar porphyroblasts in hornblende gneiss. Weinberg and Searle (1999) interpreted the late growth of poikiloblastic K-feldspar in the leucogranites of the upper Imja Khola (Khumbu Himalaya, Nepal), as products of autometasomatism. Vassallo and Vernon (2000), instead, interpreted the K-feldspar porphyroclasts of the Feral gneiss of Broken Hill (Australia) as the result of a pre- to syn-metamorphic intrusion of megacrystic granite. Vernon and Paterson (2002) interpreted the K-feldspar megacrysts in deformed granites of the Papoose Flat pluton as residual phenocrysts, not porphyroblasts. From their observations, they conclude that this explanation can be applied to most felsic augen gneisses and mylonites.

The examples studied herein come from the Strona-Ceneri Zone (lower amphibolite facies Variscan metamorphism in the south-western Italian Alps), where Ordovician granitoids intruded the protoliths of coarse- and fine-grained paragneisses (Cenerigneiss and Gneiss Minuti, respectively), as well as *banded amphibolites*, before the Variscan metamorphism. Near these metagranitoids, the *Cenerigneisses* grade into augen gneisses (*Ceneri augengneiss*), and the amphibolites grade into hornblende-bearing augen gneisses with large K-feldspar porphyroclasts (*Hbl-augengneiss*).

The origin of the *Cenerigneiss*, and the associated *Ceneri augengneiss*, is a matter of some controversy. Baechlin (1937) classified them as ''Mischgneise'', a mix of sediment and infiltrating granitic magma formed during the regional metamorphism. For Reinhard (1964) they were just metasediments. Afterward, they have been interpreted as formed by in situ anatexis of the fine-grained meta-arenites (*Gneiss Minuti*, Boriani, 1968). Later on, they have long been regarded as just metasediments (Boriani et al., 1982, 1983; Boriani et al., 1990). Their protolith was considered a sandstone-conglomerate produced by a mass-flow turbidite deposited in an accretionary prism (Boriani et al., 1995). The same interpretation was given for the Sykesville Formation in the Appalachians, which consists of metasedimentary granofels with high concentrations of quartz and feldspar. The rock resembles

granite and granite gneiss, and was known in the first half of the twentieth century as the Sykesville Granite (Drake, 1986, 1989).

However, Zurbriggen et al. (1997) re-interpreted these rocks as Ordovician intrusive rocks derived from the melting of the *Gneiss Minuti* at greater depth.

If the interpretation of a sedimentary origin of the *Ceneri augengneiss* is correct, the K-feldspar megacrysts should have grown later in the rock, either as porphyroblasts due to the recrystallization of detrital feldspar, partial melting, or due to some residual melt infiltration. If instead the *Ceneri augengneiss* is an orthogneiss, then the megacrysts are of magmatic origin. The case of the hornblende-bearing augen gneisses (*Hbl-augengneiss*) occurring in the amphibolites is different since a magmatic origin of the protolith is unlikely. If they derived from intrusive magmatic rocks, their composition should have been monzonitic. No monzonitic gneisses are present in the Serie dei Laghi. Another evidence is the gradual chemical and mineralogical transition between the *banded amphibolites* and the *Hbl-augengneiss*, in which the banding is still preserved. Because of this gradual transition Boriani and Giobbi Mancini (1972) interpreted this transformation as a metasomatic process.

In this paper, we try to envisage a genetic model that can be applied to both rock types, and which represents a different approach to the discussion of the genesis of the K-feldspar augen in some particular metamorphic rocks.

Geological setting

The area under investigation (Fig. 1) belongs to the Southern Alps Basement of the Lago Maggiore district (NW Italy), one of the so-called ''exposed continental sections'' that have yielded a lot of valuable geological information about the structure and composition of the continental crust (Fountain, 1976). The Southern Alpine domain occurs to the south of the Periadriatic Lineament, here represented by the Canavese Line (CN in Fig. 1, inset). It includes a metamorphic pre-Alpine basement, a Permian volcano-sedimentary complex and Mesozoic sedimentary cover rocks. The basement consists of an upper-amphibolite to granulite facies sequence, the Ivrea-Verbano Zone (e.g., Quick et al., 1994) and a lower-amphibolite facies unit, the Serie dei Laghi (Boriani et al., 1990).

The Serie dei Laghi consists of a meta-arenaceous unit (Strona Ceneri Zone, SCZ), which includes coarse- (*Cenerigneisses*) and fine-grained (*Gneiss Minuti*) meta-arenites, and a metapelitic unit (Scisti dei Laghi). These two units are separated by a continuous horizon, mainly consisting of *banded amphibolites*, with lenses of ultramafites, metagabbros and Grt-bearing amphibolites (Giobbi Mancini et al., 2003), called the Strona-Ceneri Border Zone (SCBZ). The SCBZ varies in thickness from less than one hundred to several hundred meters. Large lenses of metagranitoids, accompanied by metapegmatites and meta-aplites, mainly occur within or close to the SCBZ (Pezzotta and Pinarelli, 1994; Boriani et al., 1995). They are mostly granodioritic, meta-aluminous, and show calc-alkaline affinity. They have been interpreted as subduction-related, mantle-derived magmas that assimilated crustal material (e.g., Boriani et al., 1995). Radiometric ages of around 450 Ma (U–Pb concordant zircon age, Köppel and Grünenfelder, 1971) and 466 ± 5 Ma (Rb-Sr whole rock isochron, Boriani et al., 1982/1983) point to an

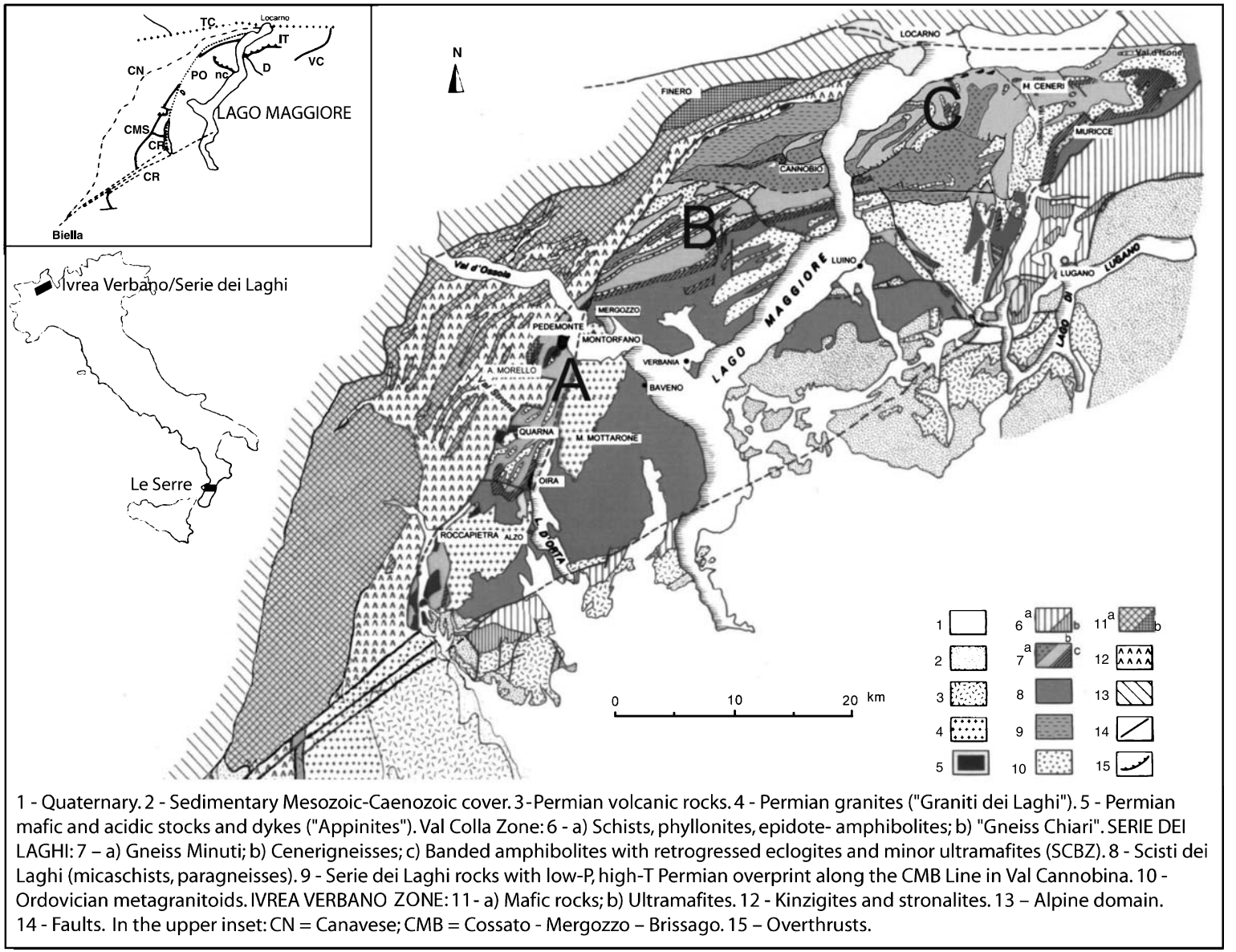

1 - Quaternary. 2 - Sedimentary Mesozoic-Caenozoic cover. 3 - Permian volcanic rocks. 4 - Permian granites ("Graniti dei Laghi"). 5 - Permian mafic and acidic stocks and dykes ("Appinites"). Val Colla Zone: 6 - a) Schists, phyllonites, epidote- amphibolites; b) "Gneiss Chiari". SERIE DEI LAGHI: 7 – a) Gneiss Minuti; b) Cenerigneisses; c) Banded amphibolites with retrogressed eclogites and minor ultramafites (SCBZ). 8 - Scisti dei Laghi (micaschists, paragneisses). 9 - Serie dei Laghi rocks with low-P, high-T Permian overprint along the CMB Line in Val Cannobina. 10 - Ordovician metagranitoids. IVREA VERBANO ZONE: 11 - a) Mafic rocks; b) Ultramafites. 12 - Kinzigites and stronalites. 13 – Alpine domain. 14 - Faults. In the upper inset: CN = Canavese; CMB = Cossato - Mergozzo – Brissago. 15 – Overthrusts.

Fig. 1. Geological sketch-map of Massiccio dei Laghi (modified after Boriani et al., 1990). The samples were collected in the areas of Lago d'Orta (A), Verbania (B), and Gambarogno (C)

Ordovician intrusion age (see discussion in Pinarelli and Boriani, 2007). Foliated pegmatite and aplite dykes occur in these metagranitoids, and in all their country rocks, mainly in the fine-grained metasediments (i.e., the *amphibolites* and the *Gneiss Minuti*), where they give rise to a sort of ''lit par lit'' (concordant with both sedimentary layering and foliation) injection. Such leucocratic dykes are rare in the *Cenerigneisses*. All these intrusive rocks underwent the same regional metamorphism as that which affected their country rocks.

Thermobarometric data from the amphibolites in the SCBZ gave temperatures in the range of 590–690 °C and pressures of 6 to 8 kbar for the main metamorphic event (Giobbi Origoni et al., 1997). $^{39}Ar/^{40}Ar$ radiometric data on Hbl, obtained from two samples of Grt-bearing *amphibolites*, yielded an age of 340 Ma (Boriani and Villa, 1997). Nineteen SHRIMP analyses on the structureless zircon rims from the *amphibolites* form a single, well-defined, concordant population with a $^{207}Pb/^{206}Pb$ age of 349 ± 13 Ma (Giobbi Mancini et al., 2004). In the adjacent Ivrea-Verbano Zone, peak regional metamorphism was reached between 273 and 296 Ma (Bürgi and Klötzli, 1990; Pin, 1990; Vavra et al., 1996; Boriani and Villa, 1997; Henk et al., 1997). The effect of this Permian event on the Serie dei Laghi is only visible near the contact with the Ivrea-Verbano Zone (Boriani et al., 1990), where a lower-pressure, higher-temperature event overprints the main Variscan associations.

Rock types, field occurrence and petrography

The following provides a brief outline of the rocks analysed in the present study. A more detailed description can be found in Giobbi Mancini et al. (2003) and Boriani et al. (2003) (reprints may be obtained on request from the authors). Table 4 reports the locations, with geographical coordinates, of the analysed samples.

Banded amphibolites

The *banded amphibolites* of the SCBZ (Fig. 2a) are strongly banded rocks with alternating dark (*fine-grained amphibolites*) and leucocratic (*leptynites*) layers, which vary from less than 1 centimetre to a few centimetres in thickness. The *fine-grained amphibolites* consist of green Hbl and Pl (An_{35-40}) and minor Bt (abbreviations according to Kretz, 1983). The modal proportions of these minerals are extremely variable owing to original variations in composition. Titanite, apatite and opaque minerals are widespread accessory minerals, zircon is rare.

The *leptynites* mainly consist of Qtz and Pl (An_{12}) with rare brown-green Bt, Hbl and small Grt grains, partially replaced by Bt (samples RB10, RB13B).

Giobbi Mancini et al. (2003) interpreted this association of *fine-grained amphibolites* and *leptynites* as an original bimodal back arc volcanic sequence consisting of alternating basaltic and rhyolitic tuffites (volcano-sedimentary deposits). The associated lenses of ultramafites, metagabbros and garnet-bearing amphibolites could represent the remnants of original olistoliths embedded in a turbiditic tuffite (Giobbi Origoni et al., 1997). The *banded amphibolites* are intersected by foliated, thin meta-aplites, which are likely correlated to the nearby Ordovician metagranitoids (Giobbi Origoni et al., 1997). At places, often near the contact with the

Fig. 2. (**a**) *Banded amphibolites*. These rocks consist of thin layers (the compass on the top left has a diameter of 1 inch) varying from basaltic to rhyolitic chemical composition. They are interpreted as the metamorphic product of a tuffite derived from a bimodal volcanic sequence. (**b**) The *banded amphibolites* grade into *Hbl augengneisses* with the increasing abundance of Kfs augen. At the stage displayed in this picture, the banded texture is still visible. Note the variable size of the Kfs crystals in the different domains. (**c**) Alternating layers of *Gneiss Minuti* and *Cenerigneisses* with sharp contacts. The layering of *Gneiss Minuti* is clearly visible

metapelites (Scisti dei Laghi), *banded amphibolites* become coarse-grained and present scattered Kfs augen (*Hbl augengneisses*, Fig. 2b). The increase in Kfs content in individuals of progressively larger size (up to 10 centimetres in length) is accompanied by the appearance of Qtz, as well as by an increase in Bt and a decrease in Hbl content. The transition from *banded amphibolites* towards *Hbl augengneisses* is accompanied by gradual changes in the composition of the individual minerals (Boriani and Giobbi Mancini, 1972): a decrease in the A^{IV} and Na contents of both Hbl and Bt as well as variation of the Pl composition from $An_{40–35}$ to $An_{26–24}$.

Meta-arenites

The sequence (Fig. 2c) comprises fine-grained, layered meta-arenites, with graded bedding evident at the scale of each thin layer (*Gneiss Minuti*), and medium- to coarse-grained meta-arenites (*Cenerigneisses*). Both contain calc-silicate nodules that show concentric zoning of mineral associations.

The dominant mineral assemblage of *Gneiss Minuti* is Qtz, Pl, Bt, and Ms. Thin meta-aplitic dykes, mostly concordant with the preserved sedimentary layering, are common. Metapegmatite dykes are often discordant with the original sedimentary layering.

The *Cenerigneisses* do not show relics of sedimentary banding. They contain Qtz, Pl, Bt, Ms and variable amounts of Kfs, Grt, Ky or (very rarely) Sil, all arranged in a typical glomeroblastic texture.

Where the contact with the Ordovician metagranitoids is well exposed, it may be seen that the *Cenerigneisses* acquire an augen texture (*Ceneri augengneiss*), in which large Kfs crystals may become very abundant. This texture is very similar to that observed in *Hbl augengneisses*. The Kfs is not always preserved, but myrmekitic Pl, in turn transformed into a fine-grained aggregate of Qtz, Pl and white mica, is always present. The Kfs also contains omoaxial inclusions of zoned Pl, as well as of Bt and Ms. The *Cenerigneisses* contain round-shaped ''enclaves'' of vein quartz and ''dioritic'' rocks, as well as mica-rich lenses. The ''dioritic'' enclaves (Qtz, Pl, Bt, Hbl and rare Grt and Ms) exhibit internal, sometimes folded, foliation distinct from that of the *Cenerigneisses*, indicating a more complex metamorphic history than that of their host rocks. The mica-rich lenses mainly contain either Ms and Grt, or Bt and Ky. If our interpretation of the Cenerigneisses as the metamorphic product of an original mass flow turbiditic deposit is correct, these lenses may represent ''soft pebbles''. In addition, zoned Ca-silicate nodules are widespread. Most of them are spheroidal and show a gradual zoning characterised by the progressive appearance, from core to rim, of Cal, Grt, Cpx, Hbl and Bt. In many cases they are disrupted by deformation, and fragments of the different shells are scattered through the rock. The major and trace element chemistry of the Ca-silicate nodules is suggestive of a diagenetic origin, although later chemical exchanges cannot be excluded.

Geochemistry

The samples for chemical analyses were selected for each rock type from a large number of specimens collected over the years, on the base of their representativeness (Boriani et al., 2003). The analytical methods are described in the Appendix. The results are reported in Table 1 and shown in Figs. 3 and 4.

Banded amphibolites

The fine-grained *amphibolites* have silica contents between 47 and 55 wt% and variable contents of K_2O, Na_2O and Sr (Fig. 3a). Their REE patterns (Fig. 4a) are rather flat, with slight enrichments in LREE ($La_N = 18–50$), moderate negative Eu anomalies ($Eu/Eu^* = 0.85–0.95$) and no HREE fractionation ($Gd_N/Yb_N = 1.1–1.2$).

Leptynites (Figs. 3a and 4b) have silica contents between 72 and 76 wt%, K_2O and Sr contents similar to those of fine-grained *amphibolites*, but higher Na_2O, Th, and LREE contents ($La_N = 60–90$), as well as pronounced negative Eu anomalies ($Eu/Eu^* = 0.4–0.7$).

The silica content of the *Hbl augengneisses* varies from 58 to 72 wt% (Fig. 3a). They can be divided into three groups: *group A* – most major and trace element

Table 1. *Whole rock chemistry of selected metasediment samples from Serie dei Laghi*

	Banded amphibolites																				
	Fine-grained amphibolites						gba	Hbl augengneisses									Leptynites				
	RB2	RB4	RB12	RB13A	RB15	VA25	VA26	A RB14	A RB20	A RB22	B RB16	B RB18	C RB19	C RBI	C RB7	C RB8	RB10	RB11A	RBI1B	RB13B	RB21
SiO_2	50.09	48.58	54.71	47.25	47.81	49.77	49.25	59.11	63.18	58.42	67.73	69.8	60.8	61.06	59.5	60.75	74.54	76.07	72.57	72.07	72.55
Al_2O_3	14.52	14.98	15.62	16.06	14.88	14.35	14.25	16.98	16.04	15.66	15.77	15.29	16.36	16.06	15.75	16.02	13.66	12.78	14.0	14.43	14.26
Fe_2O_3	2.02	1.54	1.9	0.88	1.71	3.5	2.46	0.79	1.12	2.01	0.82	0.62	0.79	0.23	0.9	0.95	0.83	0.93	0.7	0.77	0.09
FeO	9.55	9.64	8	10.25	10.18	8.85	6.93	5.6	4.29	4.88	2.21	2.07	3.56	3.18	4.07	3.31	1.93	2.09	0.97	2.13	2.53
MnO	0.2	0.19	0.19	0.21	0.21	0.23	0.22	0.12	0.1	0.14	0.06	0.06	0.07	0.07	0.09	0.07	0.06	0.03	0.07	0.05	0.05
MgO	5.69	6.31	4.57	8.31	7.31	5.57	7.43	3.97	3.02	3.71	1.49	1.26	3.73	3.15	4.22	3.54	0.51	0.22	0.62	0.62	0.89
CaO	8.87	9.9	7.88	6.57	10.35	9.3	11.13	6.23	4.5	5.18	2.86	2.56	4.09	3.61	4.28	3.86	1.99	1.77	2.54	3.2	1.97
Na_2O	3.74	2.94	3.73	2.91	2.73	3.77	2.75	3.78	4.65	4.19	3.54	3.79	3.15	3.11	3.35	3.16	5.35	5.47	5.52	4.92	4.71
K_2O	0.73	0.76	0.46	1.29	0.67	0.65	0.32	1.11	1.35	2.55	4.56	4.3	5.83	5.76	4.86	5.69	0.63	0.68	0.76	0.86	2.05
TiO_2	1.82	1.73	1.55	1.51	2.13	2.06	1.36	0.96	0.68	1.23	0.41	0.36	0.73	0.67	0.81	0.7	0.28	0.17	0.37	0.42	0.32
P_2O_5	0.27	0.19	0.26	0.17	0.21	0.25	0.15	0.2	0.16	0.25	0.43	0.15	0.38	0.28	0.44	0.41	0.06	0.02	0.08	0.08	0.08
LOI	0.67	1.17	0.84	2.69	0.91	0.42	1.17	1.22	1.28	1.7	0.59	0.48	0.97	0.66	1.34	0.87	0.85	0.67	1.16	0.99	0.77
Sc	42	43	31	44	51	46	56	24	14	24	6	5	16	12	16	15	9	6	7	12	6
V	278	291	273	285	353	338	286	163	76	150	46	42	88	64	86	73	15	7	20	11	25
Cr	98	165	40	281	181	76	186	78	55	77	35	33	174	129	180	143	u.d.l.	u.d.l.	u.d.l.	u.d.l.	18
Co	32	43	30	42	45	93	79	15	11	23	8	7	17	12	19	16	3	3	3	4	5
Ni	30	43	16	95	67	u.d.l.	u.d.l.	19	15	42	29	33	131	59	87	70	25	u.d.l.	19	u.d.l.	43
Cu	26	43	46	22	56	69	64	25	14	59	u.d.l.	u.d.l.	21	u.d.l.	16	12	14	37	31	32	u.d.l.
Zn	87	81	83	100	87	137	105	39	11	46	41	40	43	12	41	61	33	22	50	31	34
Rb	13	16	10	50	14	19	11	30	39	99	164	202	201	212	148	215	17	15	20	27	46
Sr	299	199	312	200	205	213	157	460	473	360	440	370	710	670	633	646	214	204	173	329	137
Y	36	36	37	32	42	45	35	25	17	45	16	16	19	19	22	20	53	49	33	42	35

gba garnet-bearing amphibolite. *u.d.l.* under detection limit, Major elements in wt%, trace elements in ppm

(*continued*)

Table 1 (*continued*)

	Banded amphibolites																				
	Fine-grained amphibolites						gba	Hbl augengneisses									Leptynites				
	RB2	RB4	RB12	RB13A	RB15	VA25	VA26	A RB14	A RB20	A RB22	B RB16	B RB18	C RB19	C RBI	C RB7	C RB8	RB10	RB11A	RB11B	RB13B	RB21
Zr	143	125	152	75	141	176	109	145	125	277	200	197	347	315	405	340	274	241	255	232	247
Nb	7	8	7	6	3	8	6	11	8	13	21	23	24	25	30	26	14	13	10	10	12
Ba	198	171	218	377	118	197	101	396	862	466	976	803	1861	1750	1596	1725	450	669	396	455	643
Hf	4	3.6	4.4	2.3	4	4.6	2.9	4.2	3.5	7.7	6.5	6.4	10	9.8	13	11	8.5	7.8	7.3	6.2	7.4
Ta	0.39	0.47	0.45	0.28	0.15	3.8	3,0	0.64	0.75	0.81	2.15	2.28	2.09	2.25	2.37	2.43	0.86	1.03	0.66	0.65	0.89
Pb	6	6	9	u.d.l.	6	6	5	u.d.l.	u.d.l.	11	68	97	70	26	38	85	u.d.l.	7	u.d.l.	12	8
Th	1.57	0.86	2.75	0.54	0.26	2.27	0.67	3.96	8.85	6.17	33.3	47.8	35.7	44.6	47.8	44.6	7.02	8.49	6.62	3.96	7.64
U	0.54	0.71	1.4	0.42	0.11	0.57	0.27	1.76	4.18	2.37	8.85	14.2	7.9	7.19	11.5	8.03	3.54	4.82	3.53	2.95	2.94
La	9.14	8.3	16.9	8.98	6.55	11.4	7.07	21.5	20.4	29.9	41.6	51.7	68.5	65.4	94.4	71.2	27.3	32.5	23	22.6	31.8
Ce	24.2	20.7	38.3	17.8	19.3	27.6	18.5	40.3	38.5	66	88.8	94.6	145	151	173	159	62.6	67.5	50.1	48.5	68.8
Pr	3.47	2.92	4.88	2.79	3.03	4.01	2.84	5.34	4.19	8.3	7.65	9.09	14.34	13.8	18.1	14.87	7.2	8.07	5.46	5.93	7.42
Nd	17.9	15.5	23.5	14.4	17.4	19.9	14.2	23.7	17.4	37.2	28.4	32.3	54.9	51.3	68.1	56.5	30.9	35.7	22.4	28.2	31.3
Sm	5.35	4.84	6.28	4.44	5.67	5.39	4.09	5.23	3.71	8.82	4.89	5.1	9.13	8.74	10.8	9.49	7.66	8.2	5.14	7.01	6.63
Eu	1.65	1.61	1.7	1.35	1.87	1.91	1.44	1.43	1.0	1.89	0.96	0.94	1.69	1.71	1.91	1.75	1.44	1.01	1.1	1.54	1.03
Gd	5.86	5.53	6.1	5.0	6.27	7.0	5.36	4.71	3.09	7.62	3.81	3.69	6.14	5.88	7.35	6.47	7.47	7.9	4.77	6.72	5.74
Tb	1.17	1.12	1.19	1.02	1.28	1.3	1.0	0.82	0.54	1.44	0.55	0.54	0.76	0.77	0.93	0.85	1.51	1.55	0.91	1.26	1.04
Dy	6.97	6.98	7.0	6.07	7.9	7.72	6.25	4.62	2.92	8.21	2.93	2.84	3.71	3.8	4.62	4.16	9.17	9.1	5.45	7.53	6.21
Ho	1.45	1.41	1.43	1.26	1.64	1.54	1.26	0.92	0.58	1.65	0.55	0.53	0.66	0.67	0.81	0.74	1.9	1.83	1.13	1.51	1.25
Er	4.22	4.17	4.24	3.7	4.82	4.97	3.94	2.7	1.7	4.93	1.72	1.7	2.0	2.03	2.46	2.22	6.0	5.75	3.66	4.55	3.93
Tm	0.65	0.64	0.64	0.57	0.74	0.72	0.56	0.41	0.25	0.76	0.28	0.27	0.28	0.28	0.34	0.31	0.98	0.94	0.6	0.72	0.65
Yb	4.22	4.01	4.15	3.58	4.64	4.59	3.56	2.63	1.71	4.73	1.71	1.73	1.64	1.61	1.98	1.82	6.44	6.14	4.0	5.07	4.17
Lu	0.62	0.6	0.61	0.52	0.69	0.67	0.53	0.39	0.24	0.69	0.27	0.27	0.24	0.25	0.31	0.26	0.99	0.89	0.63	0.71	0.63

gba garnet-bearing amphibolite. *u.d.l.* under detection limit, Major elements in wt%, trace elements in ppm

Table 1 (*continued*)

	Paragneisses																							
	Gneiss Minuti															Cenerigneisses					Ceneri augengneisses			
	EL14	EL15	EL17	EL19	EL21/A	EL21/B	EL24	EL26	EL27	EL28	EL29	EL22	EL23	EL25	EGC2	EL1	EL13	EL16	EL43	EGC9	EL7	EL8	EL10	EL30
SiO_2	71.58	67.95	59.94	71.33	67.34	53.67	66.89	73.49	66.78	58.69	67.41	68.5	65.44	60.19	62.97	67.04	70.84	67.66	69.16	67.1	68.46	67.07	66.54	66.26
Al_2O_3	13.11	15.41	16.57	12.69	14.26	22.00	14.72	12.55	14.82	17.94	14.73	13.67	15.04	17.56	15.8	15.32	13.61	14.74	14.97	15.05	15.35	15.09	16.23	15.04
Fe_2O_3	0.6	0.82	1.01	0.97	0.72	0.92	0.75	0.51	0.7	1.03	0.81	0.87	0.37	1.03	1.51	0.91	0.8	0.67	0.47	1.03	1.11	1.5	1.31	0.87
FeO	3.63	3.81	5.71	3.64	4.83	5.59	4.28	3.35	4.12	5.88	4.02	4.54	4.62	5.95	4.46	4.13	3.3	4.07	1.94	1.72	3.32	3.42	3.56	3.41
MnO	0.06	0.06	0.08	0.08	0.1	0.1	0.08	0.06	0.07	0.08	0.08	0.1	0.08	0.09	0.09	0.08	0.06	0.07	0.04	0.06	0.06	0.07	0.06	0.07
MgO	1.86	1.94	3.1	1.91	2.47	3.26	2.49	1.74	2.44	3.29	2.21	2.32	2.71	3.36	2.67	2.22	1.81	2.14	0.75	1.82	2.02	2.07	1.93	1.83
CaO	1.81	1.12	2.58	2.04	1.41	1.36	1.59	1.55	1.33	1.22	1.5	1.55	1.47	1.26	2.37	1.87	1.49	1.2	1.19	1.07	1.3	1.54	2.75	1.13
Na_2O	3.01	2.73	4.14	3.00	2.41	2.3	3.82	3.19	2.84	2.51	3.16	2.57	3.5	2.82	3.17	3.37	2.85	2.82	3.08	2.79	2.89	3.13	3.04	2.3
K_2O	2.59	3.57	2.7	2.4	3.5	6.05	2.86	2.45	3.5	4.77	3.2	3.05	3.12	4.23	2.21	3.11	2.93	3.32	4.86	3.98	3.61	3.61	2.86	4.53
TiO_2	0.79	0.69	0.81	0.89	0.7	0.91	0.79	0.68	0.74	0.83	0.8	0.68	0.8	0.88	0.75	0.7	0.64	0.72	0.31	0.64	0.6	0.68	0.66	0.65
P_2O_5	0.24	0.21	0.19	0.27	0.21	0.23	0.18	0.21	0.22	0.21	0.23	0.22	0.22	0.22	0.17	0.21	0.88	0.13	0.22	0.13	0.22	0.18	0.08	0.14
LOI	0.56	1.39	1.54	1.09	1.21	2.32	0.96	0.72	1.17	1.68	0.85	1.01	1.04	1.98	2.03	1.18	1.04	1.02	1.9	1.64	1.22	1.19	1.24	1.97
Sc	11	12	17	11	11	23	13	9	13	18	12	11	14	17	19	12	10	13	6	14	12	13	16	14
V	83	84	122	86	79	156	101	75	88	118	92	72	100	127	109	91	75	89	33	77	82	89	90	83
Cr	77	70	85	83	65	106	72	57	65	88	67	57	78	92	92	69	70	120	35	75	58	65	49	69
Co	12	11	23	11	17	21	16	11	12	20	14	16	16	19	151	12	10	14	151	165	10	11	13	9
Ni	55	34	52	44	48	49	43	31	32	49	38	37	45	50	40	34	110	37	17	u.d.l.	24	33	35	34
Cu	10	13	56	10	40	10	10	10	22	27	22	87	11	60	79	23	14	22	24	33	26	27	29	12
Zn	74	81	140	81	112	123	121	83	77	140	96	107	87	117	267	99	77	98	u.d.l.	83	72	97	83	55
Rb	127	130	132	82	132	173	104	94	123	197	134	120	111	167	121	175	124	140	167	144	127	132	107	168
Sr	258	177	341	226	214	204	247	239	217	153	230	236	224	181	216	230	211	171	105	177	153	163	192	147
Y	32	30	35	37	33	33	34	32	33	36	32	32	33	38	30.2	32	35	28	45	30	30	27	45	29
Zr	348	236	191	384	227	148	226	287	233	164	256	239	209	186	226	247	237	239	171	213	198	202	204	202
Nb	13	14	13	14	11	15	14	12	13	15	13	11	13	17	15.0	14	11	14	15	14	12	13	12	11
Ba	477	622	552	734	709	1670	695	625	645	766	690	620	819	748	611	642	526	505	531	940	663	743	588	928

u.d.l. Under detection limit

(*continued*)

Table 1 (*continued*)

	Paragneisses																							
	Gneiss Minuti															Cenerigneisses					Ceneri augengneisses			
	EL14	EL15	EL17	EL19	EL21/A	EL21/B	EL24	EL26	EL27	EL28	EL29	EL22	EL23	EL25	EGC2	EL1	EL13	EL16	EL43	EGC9	EL7	EL8	EL10	EL30
Hf	8.5	6.1	5.1	9.5	5.9	4	5.8	7.1	6.1	4.7	6.5	6.4	5.4	5.1	6.0	6.6	6.1	6.3	4.9	5.9	5.4	5.3	5.4	5.3
Ta	1.01	1.02	1,0	1.17	0.87	1.07	1.03	0.91	1.05	1.22	0.98	0.82	0.99	1.23	9.0	1.1	1.03	1.03	8.5	8.7	1.02	1.08	0.96	1.13
Pb	24	44	48	31	29	28	41	35	23	39	29	29	19	33	55	40	35	26	11	22	26	42	34	25
Th	15.4	11.9	11.3	19.6	11.4	15.8	11.8	13.8	13.9	14.6	12.3	10.8	11.3	14	12.7	13.5	11.5	13.7	13	10.6	11.7	13	20.3	10.5
U	3.18	3.72	3.19	3.31	2.87	3.8	2.9	2.67	3.09	3.69	3.07	3,0	2.81	3.72	2.8	3.98	3.83	3.79	3.8	4,0	4.25	3.25	2.86	3.51
La	43.8	35.7	39.6	48.3	38.1	42.1	36.8	40.6	43.3	42.3	38.8	37.3	35.5	41.6	36.6	39.8	34.5	41	27	33	34.1	35.9	37.9	27.8
Ce	88.3	72	78.2	101	75.1	87.3	75	80.8	84	84.1	78.2	72.8	72.4	84.2	70.5	78.8	68.2	82.5	58	64.8	69.2	71.6	89.6	56.7
Pr	10.16	8.26	9.18	10.86	8.75	10.04	8.84	9.22	9.85	9.79	8.91	8.42	8.47	9.96	8.43	9.18	7.74	9.31	6.3	7.67	7.9	8.34	9.54	6.56
Nd	39.2	32.3	36.2	41.1	35	38.7	35.5	35.6	39.3	38.1	35.4	33.9	33.2	39	33	35.7	31.2	36.1	25	29.8	30.6	32.6	37.9	25.4
Sm	7.74	6.63	7.34	7.89	6.92	7.74	7.19	7.15	7.8	7.88	7.09	6.95	7.01	8.03	6.24	7.61	6.31	6.95	5.8	5.82	6.23	6.61	8.27	5.14
Eu	1.43	1.21	1.66	1.48	1.29	1.46	1.43	1.33	1.46	1.41	1.46	1.36	1.39	1.49	1.37	1.36	1.19	1.28	0.8	1.32	1.21	1.21	1.08	1.09
Gd	5.98	5.23	5.9	6.14	5.49	6.04	5.73	5.49	6.04	6.15	5.55	5.55	5.53	6.47	6.23	6.03	4.97	5.42	5.9	5.65	5.04	5.15	6.62	4.33
Tb	1.02	0.93	1.06	1.04	0.99	1.04	1.01	0.93	1.04	1.04	0.96	0.96	0.98	1.16	0.95	1.04	0.93	0.86	1.3	0.86	0.94	0.87	1.27	0.75
Dy	5.66	5.31	5.81	6.12	5.42	5.81	5.64	5.14	5.68	6.13	5.36	5.2	5.39	6.61	5.41	5.71	5.54	4.66	7.8	5.06	5.05	4.66	7.06	4.55
Ho	1.04	0.98	1.11	1.18	1.07	1.1	1.08	1.01	1.05	1.14	1.02	1.0	1.03	1.24	1.02	1.04	1.04	0.9	1.5	0.99	0.97	0.86	1.45	0.88
Er	3.06	2.78	3.29	3.58	3.15	3.29	3.19	2.98	3.17	3.53	3.06	3.06	3.07	3.75	3.17	3.13	3.29	2.67	4.2	3.5	2.95	2.63	4.6	2.69
Tm	0.46	0.45	0.49	0.55	0.48	0.51	0.5	0.45	0.48	0.54	0.46	0.45	0.46	0.57	0.464	0.48	0.51	0.4	0.6	0.513	0.46	0.4	0.76	0.43
Yb	2.81	2.8	3.16	3.54	2.93	3.18	3.07	2.94	3.0	3.29	2.87	2.68	2.92	3.52	2.9	2.94	3.11	2.47	3.4	3.19	2.96	2.51	4.53	2.71
Lu	0.42	0.42	0.45	0.53	0.42	0.5	0.46	0.45	0.44	0.49	0.45	0.42	0.43	0.52	0.437	0.45	0.47	0.37	0.4	0.47	0.44	0.38	0.68	0.43

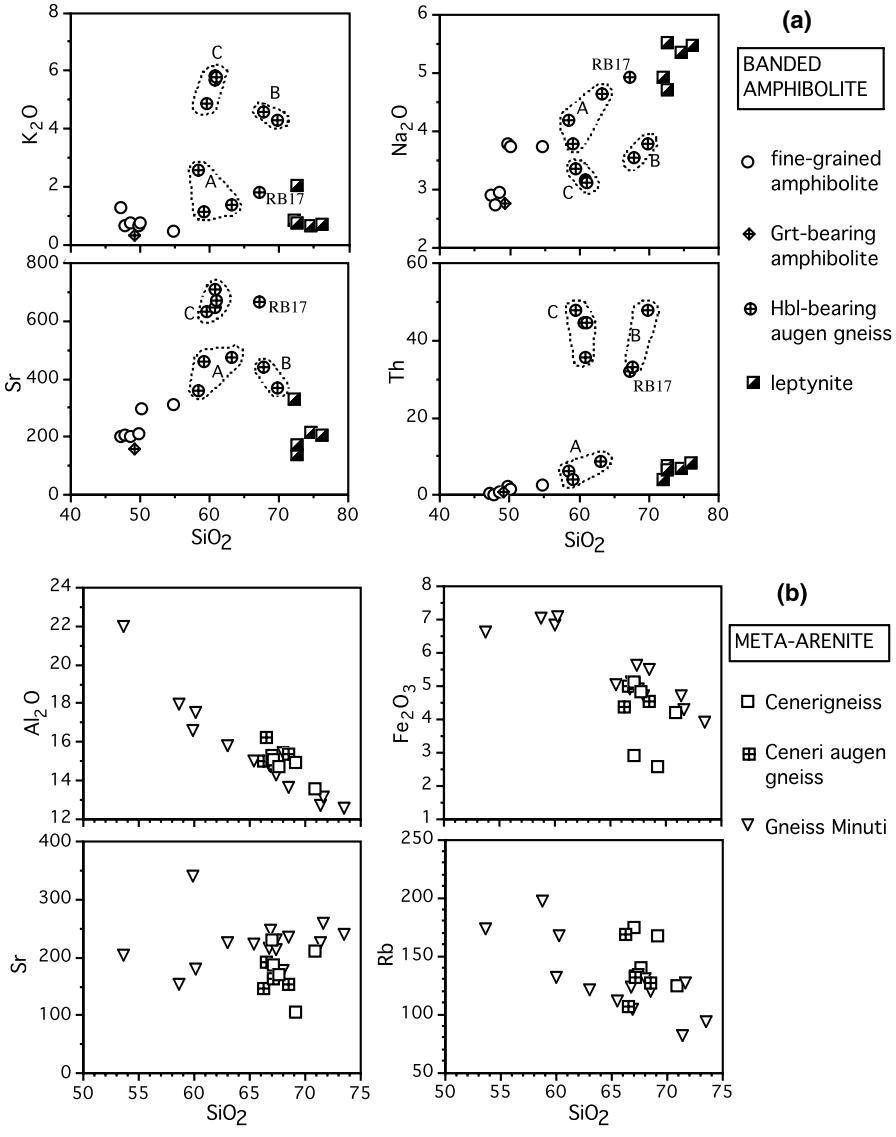

Fig. 3. Selected major and trace element vs. silica variation diagrams for the *banded amphibolites* (**a**) and meta-arenites (**b**)

contents are intermediate between the fine-grained *amphibolites* and the *leptynites*; *group B* – higher K_2O and Th, and lower Na_2O contents than group A; *group C* – on the average higher K_2O, Sr and lower Na_2O with respect to group A and B. The Th content is similar to that of group B.

Hbl augengneisses of group A exhibit more fractionated LREE patterns than the *fine-grained amphibolites* (Fig. 4c; $La_N/Sm_N = 2.1–3.5$ vs. 0.7–1.7), similar, moderately negative Eu anomalies ($Eu/Eu^* = 0.7–0.9$) and slightly negative HREE fractionation ($Gd_N/Yb_N \sim 1.4$). The REE patterns of groups B and C are very regular, with progressively higher LREE ($La_N = 113–140$ to 180–260, respectively) and lower HREE contents ($Gd_N/Yb_N \sim 3.0$ to ~ 1.8) than group A.

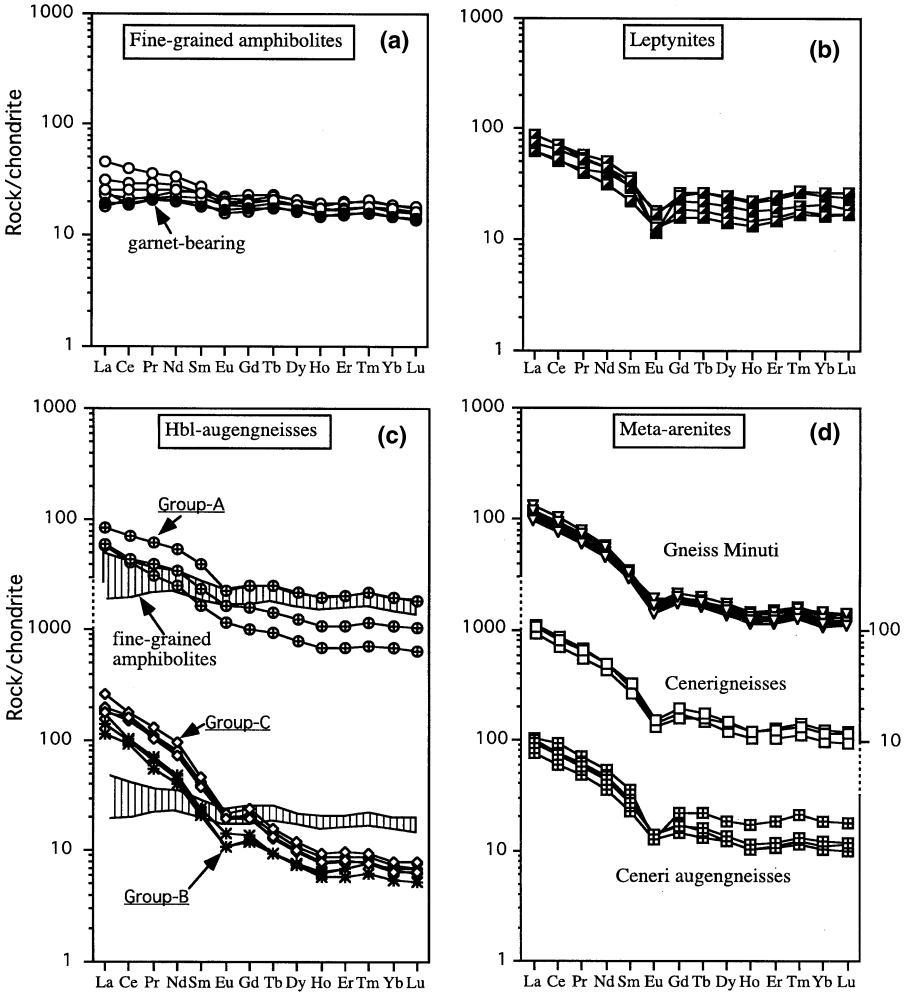

Fig. 4. Chondrite-normalised REE patterns of the *banded amphibolites* (**a**–**c**) and meta-arenites (**d**)

Meta-arenites

The *Gneiss Minuti* were accurately sampled in order to reflect their highly variable composition. Their silica content (Fig. 3b) varies widely (54–74%) and is negatively correlated with Al_2O_3, Fe_2O_3, and Rb (as well as MgO, K_2O, and Cr, not shown in Fig. 3b), as expected in strongly layered arenaceous sediments. Variations in TiO_2, CaO, Sr, Ba, La, Th, and Ta contents are instead uncorrelated with silica. The *Cenerigneisses* show large variations in trace elements, similar to those observed in the *Gneiss Minuti*, despite a restricted silica range (67–71 wt%). The composition of the *Ceneri augengneiss* mainly overlaps that of the *Cenerigneisses*.

The REE patterns of all the meta-arenites, *Ceneri augengneiss* included (Fig. 4d), are very similar to each other in terms of LREE contents ($La_N = 90$–120), negative Eu anomalies ($Eu/Eu^* = 0.60$–0.75) and HREE fractionations ($Gd_N/Yb_N = 1.2$–1.8).

Pb, Sr, and Nd isotopes

U–Pb geochronology of the Ceneri augengneiss

The analytical methods are described in the Appendix. Before interpreting zircon U–Pb age data, we used CL imagery to discriminate different internal structures of the zircon grains, as described by Hanchar and Miller (1993), Hanchar and Rudnick (1995), Kroener et al. (2000), Pidgeon et al. (2000), Corfu et al. (2003).

Caironi (1995) described the zircons of *Cenerigneisses* from the same area examined here, as showing either detrital or magmatic character, and distinguished two different kinds: (i) strongly abraded, detrital crystals, (ii) euhedral, magmatic zircons. The latter represent 22% of the entire population in the *Cenerigneisses*, 28–48% in the *Ceneri augengneiss*.

In the *Ceneri augengneiss* samples studied here, both (i) stubby, brownish zircon grains, very rich in inclusions, with rounded terminations (length-to-width 1–2:1) and (ii) long-prismatic and clear euhedral zircon crystals (length-to-width >4), are present. The stubby zircon grains show a wide variety of CL textures, from typical magmatic growth (concentric and oscillatory zoning) (Fig. 5a) to faint zoning (Fig. 5b). They also contain inherited cores, which typically have rounded shape. The long-prismatic zircons, on the contrary, never show inherited cores and are characterized by high-luminescent thin zoning (Fig. 5c). The morphology and the CL textures of the long-prismatic zircons suggest that they could derive from the crystallization of an evolved magma (Corfu et al., 2003).

Results of the U–Pb SHRIMP II analyses are reported in Table 2. Data points plot near to or on the Concordia in the $^{207}Pb/^{235}U$ vs. $^{206}Pb/^{238}U$ diagram (Fig. 6)

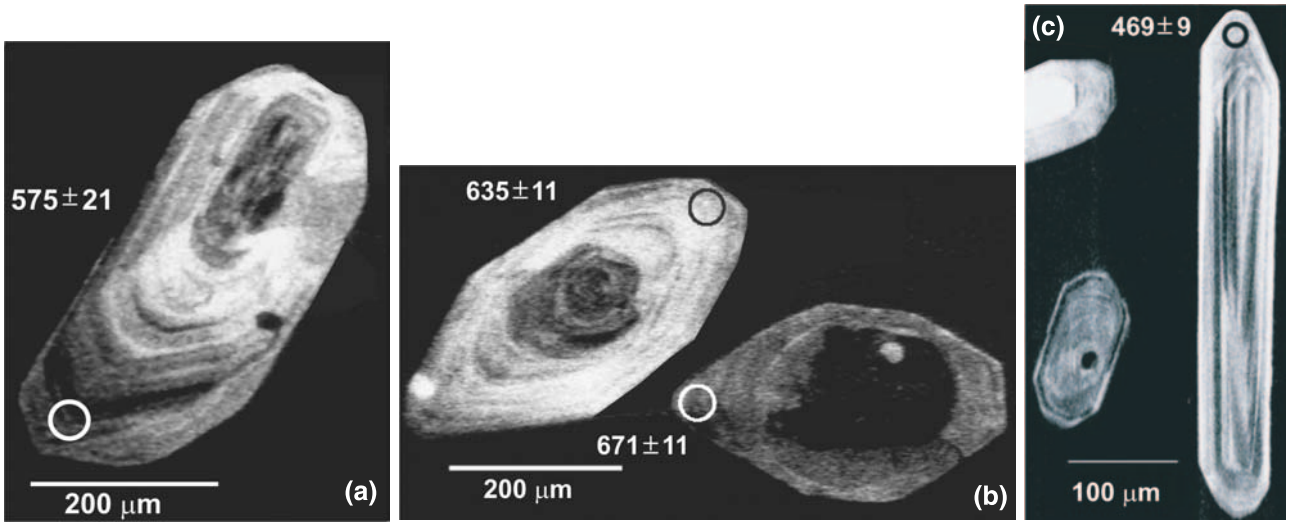

Fig. 5. CL zircon images from the *Ceneri augengneiss* samples. *Open circles* (20–25 μm) show spots of SHRIMP II analyses. (**a**) Stubby zircon grain that shows a typical magmatic overgrowth (concentric and oscillatory zoning). (**b**) Stubby zircon grain showing faint zoning. (**c**) Long-prismatic zircon characterized by high-luminescent thin zoning. For detailed description of zircon textures see text

Table 2. *U–Th–Pb SHRIMP II data for Ceneri augengneiss samples*

Spot	% $^{206}Pb_c$	ppm U	ppm Th	$^{232}Th/^{238}U$	ppm $^{206}Pb^*$	$^{206}Pb/^{238}U$ Age	$^{207}Pb/^{206}Pb$ Age	$^{207}Pb^*/^{206}Pb^* \pm \%$	$^{207}Pb^*/^{235}U \pm \%$	$^{206}Pb^*/^{238}U \pm \%$	Err. corr.
TYPE 1											
CH1-1.1	0.36	368	155	0.44	54.8	1026 ± 19	945 ± 16	0.0706 4.0	1.679 4.4	0.1726 2.0	0.446
CH1-5.1	0.03	827	455	0.57	70.0	605 ± 11	672 ± 42	0.0619 1.9	0.841 2.7	0.0984 1.9	0.691
CH1-11.1	0.04	938	105	0.12	83	632 ± 23	568 ± 17	0.0590 0.77	0.837 3.9	0.1029 3.8	0.980
CH1-18.1	0.14	955	1003	1.08	76.7	575 ± 21	632 ± 31	0.0608 1.4	0.782 4.1	0.0933 3.8	0.936
EL13-1.1	0.10	573	20	0.04	88.6	1065 ± 20	1650 ± 25	0.1014 1.3	2.513 2.4	0.1797 2.0	0.834
EL13-2.1	0.04	333	217	0.67	107	2050 ± 33	2160 ± 18	0.1347 1.0	6.95 2.1	0.3744 1.9	0.879
EL13-3.1	0.20	1447	625	0.45	129	635 ± 11	592 ± 23	0.0597 1.9	0.852 2.6	0.1035 1.8	0.683
EL13-5.1	3.90	117	88	0.78	11.1	654 ± 18	667 ± 23	0.044 4	0.65 4.2	0.1068 2.8	0.104
EL13-6.2	0.38	513	76	0.15	74.4	1003 ± 18	976 ± 25	0.0716 3.1	1.662 3.7	0.1683 1.9	0.529
EL13-7.1	0.49	493	398	0.83	46.7	671 ± 12	568 ± 19	0.0590 3.2	0.893 3.7	0.1097 1.9	0.516
EL13-8.1	0.14	1380	367	0.28	123	638 ± 11	580 ± 20	0.0593 1.6	0.851 2.4	0.1040 1.8	0.737
EL13-9.1	0.08	1125	240	0.22	106	671 ± 11	581 ± 22	0.0594 1.6	0.897 2.4	0.1096 1.8	0.747
TYPE 2											
CH1-3.1	0.36	471	56	0.12	31.5	482 ± 9	470 ± 16	0.0564 4.1	0.604 4.6	0.0776 2.0	0.436
CH1-7.1	0.16	564	63	0.12	36.6	469 ± 9	547 ± 22	0.0585 2.9	0.609 3.5	0.0755 2.0	0.564
CH1-9.1	0.40	138	43	0.32	8.42	440 ± 17	410 ± 18	0.054 6.3	0.526 7.4	0.0707 4	0.539
CH1-12.1	0.10	380	58	0.16	24.3	464 ± 17	488 ± 13	0.0569 1.9	0.585 4.3	0.0746 3.9	0.896
CH1-13.1	0.62	263	72	0.28	16	440 ± 17	421 ± 19	0.051 3.4	0.497 5.2	0.0706 3.9	0.753
CH1-14.1	0.10	804	113	0.15	51.1	460 ± 17	445 ± 28	0.0558 1.3	0.569 4	0.0739 3.8	0.948
CH1-15.1	0.29	388	31	0.08	25.9	480 ± 18	448 ± 17	0.0545 2	0.581 4.3	0.0773 3.8	0.887
CH1-16.1	0.84	259	137	0.55	15.4	429 ± 16	435 ± 21	0.0512 6.2	0.485 7.3	0.0687 4	0.541
CH1-17.1	0.13	453	181	0.41	30.3	483 ± 18	437 ± 32	0.0556 1.5	0.597 4.1	0.0778 3.8	0.935

Errors are Pb_c and Pb^* indicate the common and radiogenic portions, respectively
Error in standard calibration was 0.97% (not included in above errors but required when comparing data from different mounts)
Common Pb corrected using measured ^{204}Pb

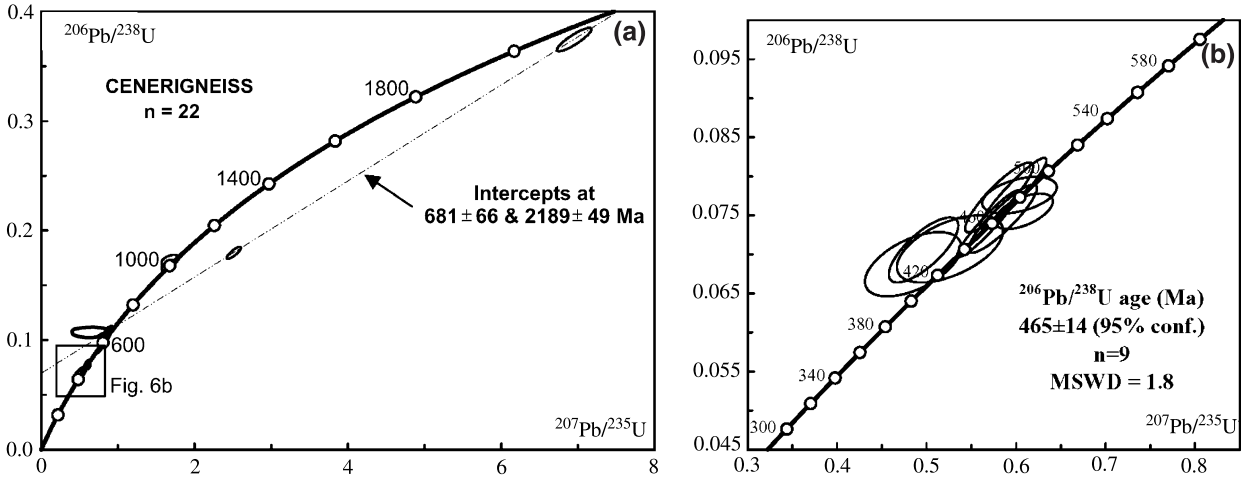

Fig. 6. (**a**) Concordia plot of SHRIMP II zircon analytical results for the *Ceneri augengneiss* samples. (**b**) detail: Concordia plot of SHRIMP II U–Pb zircon analytical results for the Ordovician zircon population (box in **a**)

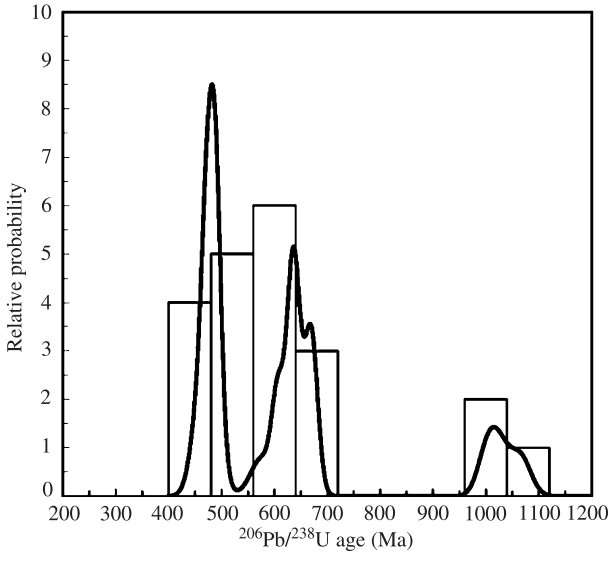

Fig. 7. Cumulative probability curves of protolith ages for the *Ceneri augengneiss* samples

and give ages that range from 0.43 to 1.0 Ga. Only two analyses (EL13-1.1, EL13-2.1) are far from the Concordia and produce a chord with intercepts at 2189 ± 49 and 681 ± 66 Ma (MSWD = 0, probability of fit = 1) (Fig. 6a).

A summary of zircon age groups is presented in a combined relative probability diagram (Isoplot; Fig. 7). Two main age populations can be distinguished: there are $^{206}Pb/^{238}U$ age peaks at 430–480 and 600–700 Ma. Two data points (EL13-6.2, CH1-1.1) give a $^{206}Pb/^{238}U$ concordant age of about 1.0 Ga.

It is important to emphasize that the long-prismatic (type 2) zircon crystals give concordant results, but with a wide age dispersion from 430 (CH1-16.1) and 440 (CH1-9.1, CH1-13.1) to 482 Ma (CH1-3.1). All the 9 data points belonging to this age population plot on the Concordia (Fig. 6b) and define a weighted mean

$^{206}Pb/^{238}U$ age of 465 ± 14 Ma at 95% confidence (MSWD = 1.8). This age is consistent with the crystallization age of the Ordovician granitoids (466 ± 5 Ma, Rb/Sr whole rock isochron, Boriani et al., 1982/83), of which the *Cenerigneiss* is the country-rock. The presence of two older age populations with different CL textures suggests inheritance from several crustal sources, with a predominance of Neoproterozoic ages. In particular, the ages around 1.0 Ga could be referred to the Kibaran orogeny in Africa (De Waele et al., 2003) or to the Grenvillian orogeny (e.g., in Scotland, Newfoundland etc.), whereas the age peaks at 600–700 Ma may be attributed to the Pan-African event (Condie, 1997).

Sr, Nd, and Pb isotope characteristics

The results of Sr, Nd, and Pb isotope analyses are reported in Table 3. The analytical methods are described in the Appendix.

Table 3. *Sr, Nd, and Pb isotope data on selected metasediment samples from Serie dei Laghi*

Sample	Sm ppm	Nd ppm	$^{143}Nd/^{144}Nd \pm 2\sigma$	Rb ppm	Sr ppm	$^{87}Sr/^{86}Sr \pm 2\sigma$	Pb ppm	U ppm	Th ppm	$^{206}Pb/^{204}Pb$	$^{207}Pb/^{204}Pb$	$^{208}Pb/^{204}Pb$
Banded amphibolites												
Fine-grained amphibolites												
RB13A	4.7	16	0.512857 ± 33	41	207	0.706930 ± 82	6	0.4	0.5	18,695	15,609	38,220
RB15	4.8	17	0.512970 ± 32	14	212	0.706061 ± 19	6	0.1	0.3	17,956	15,528	37,807
VA25	5.4	19	0.512729 ± 17	16	211	0.706040 ± 35	6	0.6	2.3	18,696	15,671	38,419
Garnet-bearing												
VA26	4.5	15	0.512730 ± 24	10	165	0.705265 ± 82	5	0.3	0.7	18,424	15,707	38,442
Hbl augengneisses												
RB1	7.4	43	0.512143 ± 20	225	728	0.714661 ± 20	26	7.2	44.6	18,574	15,630	38,789
RB16	5.6	32	0.512192 ± 46	163	427	0.713194 ± 35	68	8.9	33.3	19,573	15,685	38,817
Leptynites												
RB1O	7.6	32	0.512655 ± 86	36	225	0.706490 ± 18						
RB11a	7.5	33	0.512596 ± 6	14	209	0.706570 ± 15						
RB21	6.5	30	0.512567 ± 43	20	138	0.714310 ± 11						
Paragneisses												
Gneiss Minuti												
EL17	6.7	34	0.512078 ± 20	130	349	0.719021 ± 61	48	3.2	11.3	18,572	15,688	38,642
EL19	7.7	42	0.511987 ± 15	88	238	0.717547 ± 37	31	3.3	19.6	18,985	15,711	39,933
EL21A	6.4	32	0.512047 ± 23	130	225	0.720060 ± 74	29	2.9	11.4	18,919	15,686	39,454
EGC2	6.6	33	0.512098 ± 20	121	225	0.719960 ± 28	55	2.8	12.7	18,654	15,703	38,994
Cenerigneisses												
EL13	5.7	29	0.512059 ± 30	124	221	0.721475 ± 11	35	3.8	11.5	18,876	15,692	38,887
EGC9	5.2	27	0.512256 ± 34	133	187	0.723274 ± 12	22	4.0	10.6	18,695	15,661	38,744
Ceneri augengneisses												
EL8	5.8	30	0.512013 ± 28	149	177	0.725580 ± 33	42	3.3	13.0	18,716	15,714	39,264
EL30	5.2	26	0.512106 ± 15	163	150	0.725839 ± 11	25	3.5	10.5	18,790	15,679	38,682

Table 4. *Locations of the analysed samples*

Sample	Lithology	Sheet	Geographical coord.
EL8	Ceneri augengneiss	32TMR	67009950
EL30	Ceneri augengneiss	32TMR	66009750
EL7	Ceneri augengneiss	32TMR	66329940
EL10	Ceneri augengneiss	32TMR	71701035
EGC9	Cenerigneiss	32TMR	60509450
EL43	Cenerigneiss	32TMR	67259818
EL13	Cenerigneiss	32TMS	77310031
EL16	Cenerigneiss	32TMS	77310032
ELI	Cenerigneiss	32TMR	66959925
EL14	Gneiss Minuti	32TMS	77310030
EL15	Gneiss Minuti	32TMS	77310030
EL19	Gneiss Minuti	32TMS	84700730
EL21A	Gneiss Minuti	32TMR	81000306
EL24	Gneiss Minuti	32TMS	81700240
EL26	Gneiss Minuti	32TMS	81720230
EL27	Gneiss Minuti	32TMS	81750225
EL29	Gneiss Minuti	32TMS	81750010
EGC2	Gneiss Minuti	32TMR	68149826
EL22	Gneiss Minuti	32TMS	81000306
EL23	Gneiss Minuti	32TMS	81300250
EL17	Gneiss Minuti	32TMS	82700660
EL21B	Gneiss Minuti	32TMS	81000306
EL28	Gneiss Minuti	32TMS	81750225
EL25	Gneiss Minuti	32TMS	81710230
VA26	Garnet bearing amphibolite	32TMR	52168612
VA25	Banded amphibolite	32TMR	51857590
RB2	Banded amphibolite	32TMR	51857590
RB4	Banded amphibolite	32TMR	80859682
RB12	Banded amphibolite	32TMR	69839850
RB13A	Banded amphibolite	32TMR	69959830
RB15	Banded amphibolite	32TMR	69879765
RB10	Leptynite	32TMR	69839850
RB11A	Leptynite	32TMR	69839850
RB11B	Leptynite	32TMR	69839850
RB13B	Leptynite	32TMR	69959830
RB21	Leptynite	32TMR	69709730
RB1	Hbl augengneiss	32TMR	51927610
RB7	Hbl augengneiss	32TMS	80200007
RB8	Hbl augengneiss	32TMR	51627572
RB14	Hbl augengneiss	32TMR	69899770
RB16	Hbl augengneiss	32TMR	69899770
RB18	Hbl augengneiss	32TMR	69899770
RB19	Hbl augengneiss	32TMR	69899770
RB20	Hbl augengneiss	32TMR	69899770
RB22	Hbl augengneiss	32TMR	66089235

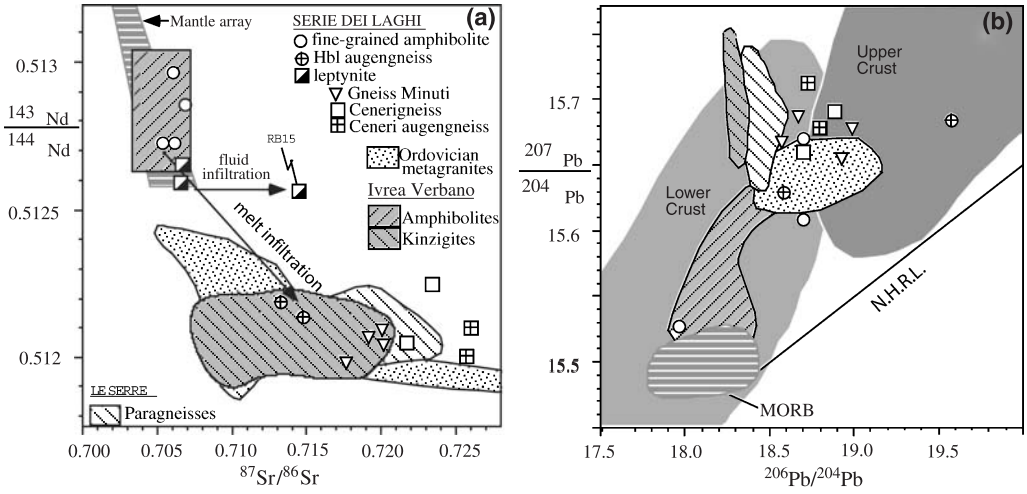

Fig. 8. $^{143}Nd/^{144}Nd$ vs. $^{87}Sr/^{86}Sr$ (**a**) and $^{207}Pb/^{204}Pb$ vs. $^{206}Pb/^{204}Pb$ (**b**) diagrams plotting the studied metasediments from Serie dei Laghi. The fields of the Ordovician metagranitoids and the metasediments from other Italian crustal sections, in which both lower and upper crust are exposed (Ivrea Verbano and Le Serre, Calabria, S-Italy), are also plotted. Data source: Le Serre: Caggianelli et al. (1991); Ivrea Verbano: Cumming et al. (1987), Pin (1990), Voshage et al. (1987, 1990); Ordovician metagranitoids: Pezzotta and Pinarelli (1994). Upper crust, Lower crust and MORB fields are from Zartman and Doe (1981); N.H.R.L. from Hart (1984)

The studied metasediments yield distinct Sr-Nd isotope patterns in the $^{143}Nd/^{144}Nd$ vs. $^{87}Sr/^{86}Sr$ diagram (Fig. 8a): the *fine-grained amphibolites* and *leptynites* plot in the field of mantle-derived rocks. The *Hbl augengneisses* plot in the field of crustal rocks, along with *Cenerigneisses* and *Gneiss Minuti*.

On the Pb-Pb diagram (Fig. 8b), the *fine-grained amphibolites* and *Hbl augengneisses* show highly variable Pb isotopes, which scatter from crustal- down to MORB-like values. The *Cenerigneisses* and *Gneiss Minuti* have more uniform Pb isotope ratios and plot at the transition between the upper and lower crust fields.

A comparison of the current data set to the isotope characteristics of other Italian crustal sections in which both lower and upper crust are exposed (Ivrea Verbano and Le Serre, Fig. 8) shows that the *fine-grained amphibolites* and *leptynites* from the SCBZ are isotopically similar to the amphibolites from the Ivrea Verbano zone. The *Hbl augengneisses*, *Gneiss Minuti* and *Cenerigneisses* have progressively lower $^{143}Nd/^{144}Nd$ and higher $^{87}Sr/^{86}Sr$. Their Sr-Nd isotope ranges overlap with the field of metasediments from both Ivrea Verbano and Le Serre, as well as that of the Ordovician metagranitoids. The *Ceneri augengneisses*, instead, show distinctly higher Sr isotope ratios, only reached by the Ordovician metagranitoids.

Discussion

The Cenerigneisses: metasediments or metaintrusives?

Zurbriggen et al. (1997) regarded the *Cenerigneisses*, *Ceneri augengneiss* included, as Ordovician intrusive rocks (which they called ‘‘Ceneri granitoids’’) origi-

nated by partial melting at greater depth at an estimated temperature of about 850 °C, and then intruded in the overlying rocks. This melting could not have occurred ''in situ'', because the outcropping SCZ rocks never seem to have been heated above temperatures of 700 °C. In the model of Zurbriggen, the *Cenerigneisses* and *Ceneri augengneiss* would represent melts segregated from a parent rock similar to the *Gneiss Minuti*. However, the strong similarity of the chemical composition of the *Cenerigneisses*, *Ceneri augengneiss*, and *Gneiss Minuti* conflicts with the well-known diversity in the geochemical patterns of partial melts and parent rocks. The REE patterns of such melts are complementary to those of the respective residual rocks, and show for the most part positive Eu anomalies (Sawyer, 1986; Barbey et al., 1996; Otamendi and Patino Douce, 2001). The REE patterns of the *Cenerigneisses*, *Ceneri augengneiss*, and *Gneiss Minuti*, instead, are almost identical (Fig. 4d), exhibit no positive Eu anomalies and resemble the typical Phanerozoic clastic sediment patterns (Taylor and McLennan, 1985). Even in the case of high degrees of melting, residual garnet would cause strong depletion of HREE in the melt. For instance, 60% melting (the maximum value for Al-rich metagreywackes according to Vielzeuf and Montel, 1994; Montel and Vielzeuf, 1997) of *Gneiss Minuti* would produce a liquid with La/Lu of 120 to 160 (5–15% garnet in the residuum; partition coefficients from Harris et al., 1992; Watt and Harley, 1993), higher than those of *Cenerigneisses* (70–110).

One might speculate that *Cenerigneisses* and *Ceneri augengneiss* represent a metamorphosed mesocratic diatexite formed when metasedimentary rocks melted sufficiently to undergo bulk flow or magma flow, but did not experience significant melt-residuum separation (Milord et al., 2001). In this case, the mica-rich lenses could be interpreted as schlieren, although they differ from those described by Milord and Sawyer (2003), which are concentrations of melanocratic minerals, namely biotite. However, this interpretation conflicts with the observation that *Cenerigneisses* and *Gneiss Minuti* are sometimes interlayered, without the appearance of any evidence of igneous contacts, like grain size variations or presence of leucocratic veins. Both features are instead very common at the contacts of the Ordovician metagranitoids.

The *Cenerigneisses* contain zoned calc-silicate nodules that may represent former dolomite concretions in sandstones, as well as mica-rich lenses interpreted as original soft pebbles. These features, along with type-1 zircon ages of the *Ceneri augengneisses* from 575 Ma to about 1.0 Ga, support the hypothesis of a sedimentary origin for their protolith, in agreement with Boriani et al. (1995), who interpreted the *Cenerigneisses* as a sandstone-conglomerate produced by a mass-flow turbidite. One of the arguments put forward by Zurbriggen et al. (1997) to support the intrusive nature of the *Cenerigneisses* is the presence of purported xenoliths of *Gneiss Minuti*. Our field observations do not confirm that presence. Those ''xenoliths'' are actually fragments of the outer shell of disrupted, zoned calc-silicate nodules.

In conclusion, both the geochemical and petrographic data are at odds with the hypothesis that the protolith of *Cenerigneisses* and *Ceneri augengneiss* is an intrusive anatectic rock derived from *Gneiss Minuti*, or from a rock similar to them, by partial melting. In addition, the *Ceneri augengneiss* share many similarities with the *Hbl augengneisses*, which occur within the *banded amphibolites*. If an anatec-

tic model could explain the genesis of the *Ceneri augengneiss*, it should also account for the origin of the *Hbl augengneisses*. Instead, the *Hbl augengneisses* have much lower Nd and higher Sr isotope ratios than their likely protolith (the *fine-grained amphibolites*), as well as the *Ceneri augengneiss* have higher Sr isotope ratios than *Gneiss Minuti*. Thus, whatever process generated both types of augen-gneisses, it implies the addition of other components with different Sr and Nd isotope ratios to both the *Cenerigneisses* and the *fine-grained amphibolites.*

The melt infiltration model

The occurrence of both the *Ceneri-* and *Hbl-augengneisses* near the contact with the Ordovician metagranitoids, along with the isotope evidence for addition of isotopically evolved components, are suggestive of a melt infiltration process. In the coarse-grained rocks, residual fluid-rich melts from the Ordovician magmatism pervasively infiltrated the protoliths of the *Hbl augengneisses* and *Ceneri augengneisses*. In the fine-grained rocks (*fine-grained amphibolites* and *Gneiss Minuti*), larger, discrete melt accumulation occurred in extensional or transpressional domains such as boudin necks, veins, and ductile shear zones, forming a network of aplitic veins and pegmatitic dykes, (similar to the textures observed by Wohlers and Baumgartner, 2004). Such a process would have to be pre-Variscan because all the considered rocks are metamorphic.

The presence of permeability and its variations from the surface to at least 30 km depth in the continental crust has been known for a number of years (e.g., Manning and Ingebritsen, 1999). In sedimentary rocks, pressurised water filling the pores maintains permeability. During contact metamorphism, overpressure of the fluid phase generated by devolatilization reactions during heating keeps the host rock porosity open. Fluid flow occurs through a medium that is already fluid saturated (Cartwright, 1997). As a rule, fluid flow is predominantly vertical, but local heterogeneities in permeability, or strong thermal or pressure gradients, may foster deviations from this trend. Chemical variations during infiltration appear to proceed in waves, due to the propagation of the high-porosity zone (Nakamura and Watson, 2001), giving rise to ''infiltration fronts''. The type of front developed (diffuse or sharp, continuous or differential) is a function of the particular element considered, pressure (Sibson, 1996) and total ion concentration (chromatographic model). Accordingly, for a given distance from the beginning of infiltration, the concentrations of different elements in the infiltrated rock may vary to a different extent, depending on the front developed.

Infiltration models generally apply to infiltration of a fluid into a rock (Hofmann, 1972; Baker and Spiegelman, 1995). However, Watson (1982) made a series of ''melt infiltration'' experiments demonstrating that under some circumstances, magma bodies will tend to disperse by infiltrating their host rocks. Later on, Guy (1993) revised the theory of infiltration-metasomatism and extended its application to the case in which a magmatic liquid migrates into a solid porous rock. Examples of infiltration of leucogranitic melts into their host rocks were recently provided by Weinberg and Searle (1999), Baumgartner et al. (2001), Hasalova et al. (2006). Melt infiltration typically leads to asymmetric chemical variation patterns. The direction of the resulting chemical variations is generally

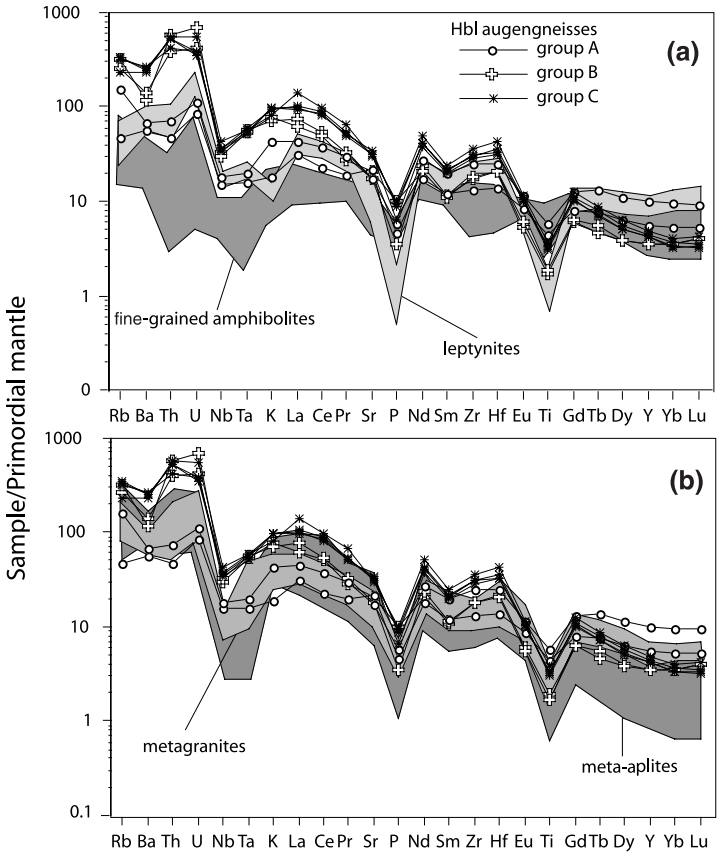

Fig. 9. Hygromagmaphile-element spidergrams normalised to the primordial mantle (Sun and McDonough, 1989) showing the studied amphibolites (**a**), along with the Ordovician metagranites and meta-aplites (Pezzotta and Pinarelli, 1994) (**b**)

unpredictable because of ‘‘bypassing’’ of impermeable layers by permeable pathways and non-pervasive flow (McCaig and Knipe, 1990; Gerdes et al., 1995). Such circumstances may explain the uneven distribution of both the *Ceneri augengneiss* and *Hbl augengneisses* near the Ordovician plutonic rocks.

Testing the infiltration model with geochemistry

The meta-arenites are poorly suited to test the chemical effects of the infiltration process because of the chemical similarity between *Cenerigneisses*, *Gneiss Minuti*, *Ceneri augengneisses*, and Ordovician intrusive rocks (see Fig. 10). For this reason we selected the *Hbl augengneisses* to first test the infiltration model. Under the hypothesis that their protolith had a composition belonging to the *fine-grained amphibolite – leptynite* sequence, the group A samples would represent the less infiltrated sediments (Fig. 3a). The progressive enrichment in K_2O, Ba and incompatible elements of groups B and C could derive by infiltration of increasing amounts of the residual hydrous melts. The spider diagrams in Fig. 9 support this interpretation. The patterns of group A *Hbl augengneisses* are similar to those of

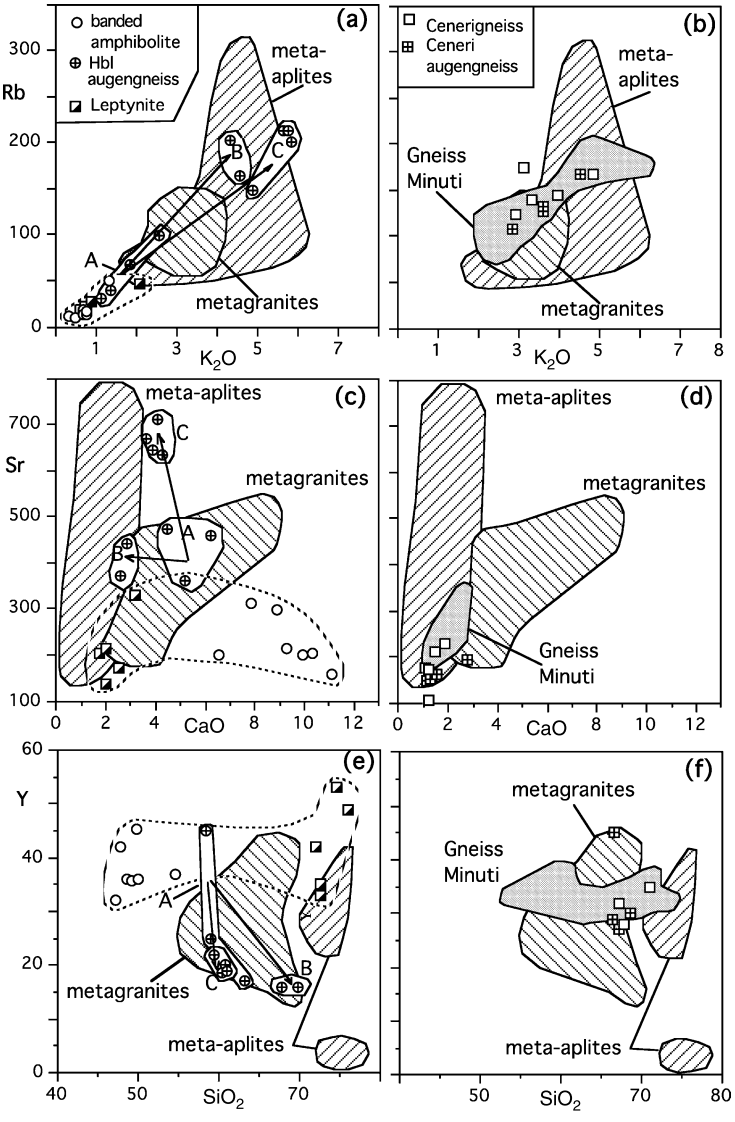

Fig. 10. Selected inter-element variation diagrams of the studied metasediments (amphibolites: **a**, **c**, **e**; meta-arenites: **b**, **d**, **f**) along with the Ordovician metagranitoids (data from Pezzotta and Pinarelli, 1994). The hypothetical paths of melt infiltration (*arrows*) point to the composition of the Ordovician meta-aplites

the *leptynites* (Fig. 9a), while the patterns of groups B and C mimic those of Ordovician meta-aplites, with a strong increase in LILE and LREE (Fig. 9b). However, Ba, Th, U, and Zr contents of groups B and C are hardly supported by either meta-aplitic or metagranitic melts.

The inter-element diagrams (Fig. 10) confirm that the rocks of group B and C were infiltrated to a larger extent with respect to those of group A. Indeed, the strong enrichments in Rb, K_2O, Sr and depletions in Y and CaO of the group B and C require the addition of larger amounts of aplitic liquids than group A, in order to be reached (Fig. 10a, c and e).

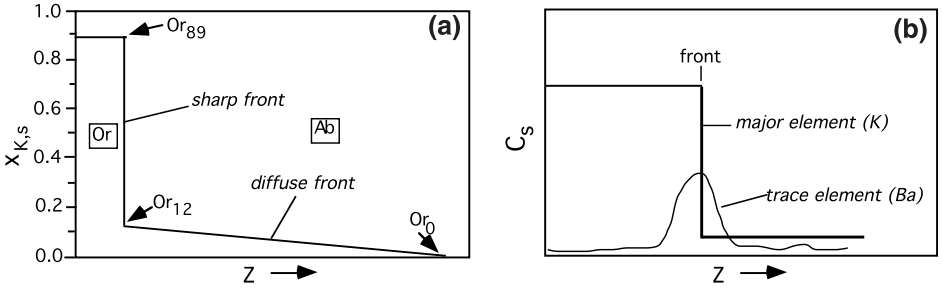

Fig. 11. Infiltration fronts (modified after Hofmann, 1972; Guy, 1993). Z = distance from the origin of infiltration in the direction of flow (equivalent to time *t*) (**a**) $X_{K,s} = C_{K,s}/(C_{K,s} + C_{Na,s})$ = molar fraction of the orthoclase component. Front development in an alkali feldspar having $X_{K,s} = 0$, after infiltration of a fluid of $X_{K,f} = 0.5$. A feldspar Or_{89} will replace the original Ab_{100} as the fluid advances through the rock. A sharp front will develop at high K concentrations. As $X_{K,f}$ decreases with increasing distance from the origin of infiltration, a diffuse front develops which intersects the sharp front at Or_{12}. (**b**) C_s = concentration of a particular element in a solid rock. Front development in a solid rock infiltrated by a fluid. The sharp front of a major element (for instance K) produces a localised increase in the concentration of a trace element (for instance Ba) of low uniform content at time zero

To estimate the amount of added liquid necessary to account for the observed element variations within the *Hbl augengneisses*, we attempted modelling the infiltration process, in first approximation, as binary mixing. We started from a rock having the average composition of the group A samples (the less infiltrated) mixed with an Ordovician aplitic melt, to give the average composition of the group C samples (the most infiltrated). The results obtained indicate about 75–80% added liquid for the balance of Rb, Sr and Y, but the high contents of K, Ba, Th, U and Zr cannot be reached via the addition of neither aplitic nor granitic liquid.

The extreme enrichments of K and Ba may be accounted for by the replacement of plagioclase by microcline, following the reasoning of Hofmann (1972). Let us consider the hypothetical case (Fig. 11a) of a fluid having a K molar fraction ($X_{K,f}$) of 0.5 (a value observed in many Ordovician aplites) that infiltrates an albitic plagioclase ($X_{K,s} = 0$). The final K (and hence its substituent, Ba) molar fraction in the infiltrated rock after replacement, near the origin of infiltration, may reach the value of 0.89, far higher than that of the infiltrating liquid. Concerning Ba, an additional further increase may be due to the propagation mode of chemical variations. Indeed, following Guy (1993) the propagation of a front pertaining to a major element, for instance K, can produce a localized increase in the concentration of a trace element of uniform low content before infiltration, for instance Ba (Fig. 11b).

As regards to the enrichment of Th, U, and Zr in the samples of group B and C, according to Watson (1982), incompatible trace elements from the wall rocks may enter the infiltrating liquid without subsequent removal by crystallizing minerals, thus resulting in a net enrichment in the incompatible-element content of the melt.

Regarding the isotopes, the *Hbl augengneisses* show lower Nd and higher Sr isotope ratios than the fine-grained amphibolites and plot in the field of the

Ordovician metagranitoids (Fig. 8a), thereby lending support to the infiltration model. The Sr isotope enrichment of *leptynite* RB15, at variance with the nearly constant $^{143}Nd/^{144}Nd$, suggests the prevalence of aqueous fluids that, unlike the residual magmatic liquids, carry a high amount of Sr, but no Nd.

Taking the *Ceneri augengneisses* into examination, their geochemical patterns are similar to those of the *Cenerigneisses* and *Gneiss Minuti* (Figs. 3b and 4d), and extensively overlap those of the Ordovician intrusives (Fig. 10b, d, and f). This observation is in agreement with the hypothesis that infiltrated melts belonged to the Ordovician magmatism. In contrast to the widespread chemical uniformity, substantial isotope variations are present within the meta-arenites. First, the *Ceneri augengneiss* have higher Sr isotope ratios than both the *Cenerigneisses* and the *Gneiss Minuti*, and more generally, higher than those of known Phanerozoic metasediments from other Italian crustal sections (Ivrea Verbano and Le Serre; Fig. 8a). Ordovician metagranitoids, on the other hand, do reach Sr isotope ratios high enough to produce the displacement observed in the *Ceneri augengneiss*. Second, the *Ceneri augengneisses* contain two zircon populations that yield two contrasting age groups: 0.57–1.0 Ga, which may represent the ages of detrital zircons derived from the erosion of late-Proterozoic to Pan-African crust, and 466 ± 13 Ma, which coincides with the emplacement age of the Ordovician granites.

Concluding remarks

The above geological, chemical, and isotope evidence has led us to interpret the *Ceneri augengneisses* and *Hbl augengneisses* as the result of infiltration of a residual hydrous magma into the protolith of both the meta-arenites and the amphibolites, at the time of Ordovician granitoid emplacement. Pressurized fluids saturating the host rocks would have provided the required porosity. A model of infiltration of melts having the composition of the Ordovician meta-aplites can account for the observed chemical and isotope patterns. This process would therefore have taken place before the Variscan regional metamorphism in the Serie dei Laghi.

The metasediments of the Serie dei Laghi provide a good example of how a change in mineralogical, chemical and isotopic composition of metamorphic rocks not necessarily derive from regional metamorphism. Our geological and geochemical data point to a pre-metamorphic transformation, induced in the sedimentary protolith by the fluid-rich residual melts of the Ordovician plutonism. In our opinion such a model can further improve our understanding of some heretofore inexplicable gradual transitions from metasediments to orthogneiss-like rocks in metamorphic terranes.

Acknowledgements

We are indebted to Dr. Liu Dunyi for use of the SHRIMP II facilities at the Beijing Institute of Geology of the Chinese Academy of Geological Sciences, SHRIMP Centre. We also wish to thank A. Möller and an anonymous referee for their helpful comments on the manuscript.

This work has been carried out with the support of a MURST – COFIN grant (1998 and 2000).

Appendix – Analytical methods

Major elements were analysed using the lithium metaborate/tetraborate fusion ICP whole rock package, and trace elements with the ICP-MS package, at Actlabs Laboratories (Canada). Quality controls (reproducibility and analytical error) with international geostandards were performed during sample analysis. The standard deviation for trace elements was 2–10% at the 10-ppm level, and 2–5% at 100 ppm. The FeO content was determined via the volumetric method. The results of chemical analyses are reported in Table 1.

The Sr, Nd, and Pb isotope ratios were determined at the Institut für Geologie, Universität Bern (Switzerland) on a Nu Instruments ICP-Mass Spectrometer (Schoenberg et al., 2000). The measured Sr isotope ratios were adjusted to a value of 0.71025 for the NBS 987 standard. Nd isotope ratios were normalised to $^{146}Nd/^{144}Nd = 0.7219$. The external reproducibility of NBS 987 and La Jolla standards were respectively ± 20 and ± 35 ppm (95% c.l.) over the analysis period. The external reproducibility values of the NBS 981 standard for the $^{206}Pb/^{204}Pb$, $^{207}Pb/^{204}Pb$ and $^{208}Pb/^{204}Pb$ ratios were respectively 16.937 ± 3, 15.493 ± 3 and 36.701 ± 6 (95% c.l.) over a 6-month period. Details on chemical separation can be found in Pettke and Diamond (1995), Frei et al. (1997), Kleinhanns et al. (2002).

Rb, Sr, Sm, and Nd contents were determined by isotope dilution (ID). The resulting uncertainties are below 0.3% for $^{87}Rb/^{86}Sr$, and 0.5% for $^{147}Sm/^{144}Nd$. The results of the isotope analyses are reported in Table 2. The small differences between the Rb, Sr, Sm and Nd concentration values reported in Tables 1 and 2 are due to the different analytical methods used (ICP/MS vs. ID). In order to avoid the risk of compromising the self-consistency of the chemical data, we have omitted the ID values from Table 1. Accordingly, the figures representing the chemical data are based entirely on Table 1.

Zircons were separated from the rock samples using standard crushing, Frantz isodynamic separator, and heavy-liquid techniques, and purified by handpicking under binoculars. They were mounted together with standard zircons (TEMORA – TEM) in epoxy resin, and polished to reveal their midsections. The zircon grains were also photographed in reflected and transmitted light. Cathodoluminescence (CL) imaging of zircon grains was carried out using a scanning electron microprobe at the Beijing Institute of Mineral Resources (CAGS). The mount was then cleaned and gold-coated.

U-Th-Pb analyses were made using an Australian Scientific Instruments Pty Ltd SHRIMP II at the Beijing Institute of Geology (CAGS). A 7-nA mass-filtered O_2- primary beam was focused to sputter a 15–20 μm diameter area with positive ion extraction. Detailed analytical procedures are similar to those described by Compston et al. (1984) and Nelson (1997).

The standard TEMORA zircons ($^{206}Pb/^{238}U$ age of 417 Ma) of RSES (Research School of Earth Sciences, Canberra) were used in calibration of inter-element fractionation, and U, Th and Pb concentrations were determined using the standard Sri Lankan gem zircon SL13 ($^{206}Pb/^{238}U$ age of 572 Ma, U = 238 ppm).

The Pb/U ratios of unknown samples were corrected using the ln(Pb/U)/ln(UO/U) relations as measured in standard SL13. Both $^{206}Pb/^{238}U$ and $^{207}Pb/$

^{206}Pb ages quoted in the text are the weighted mean at the 95% confidence level. All reported $^{206}Pb/^{238}U$ ages have been corrected by the ^{204}Pb technique (Compston et al., 1984), assuming a Broken Hill common Pb composition. Uncertainties in age calculations depend on both counting statistics and the additional effect of the common Pb correction. The analytical data were initially reduced using the computer program SQUID 1.02 (Ludwig, 2001b) and both concordia diagrams and histograms were plotted using Isoplot/Ex (Ludwig, 2001a).

References

Baechlin R (1937) Geologie und Petrographie des Monte Tamaro-Gebietes (Suedliches Tessin). Schweiz Mineral Petrogr Mitt 17: 1–79

Baker J, Spiegelman M (1995) Modelling an infiltration-driven geochemical front. Earth Planet Sci Lett 136: 87–96

Barbey P, Brouand M, Le Fort P, Pecher A (1996) Granite-migmatite genetic link: the example of the Manaslu granite and Tibetan Slab migmatites in central Nepal. Lithos 38: 63–79

Baumgartner LP, Clemens RM, Putlitz B, Roselle GT, Wenzel TU (2001) Fluid and melt movement in contact aureoles. 11th Annual Goldschmidt Conference

Boriani A (1968) Il settore meridionale del gruppo del Monte Zeda (Lago Maggiore, Italia): Osservazioni petrogenetiche. Schweiz Mineral Petrogr Mitt 48: 175–188

Boriani A, Burlini L, Caironi V, Colombo A, Giobbi Mancini E, Tunesi A, Zappone A (2003) The abundance of 54 elements and petrovolumetric models of the crust in Val d'Ossola – Lago Maggiore and Valtellina (site 2). Acc Naz Delle Scienze (detta dei XL) Scritti e Documenti 32: 97–162

Boriani A, Giobbi Mancini E (1972) The feldspathized amphibolites of the Strona Ceneri Zone. Boll Soc Geol Ital 91: 655–681

Boriani A, Giobbi Origoni E, Pinarelli L (1995) Paleozoic evolution of southern Alpine crust (Northern Italy) as indicated by contrasting granitoid suites. Lithos 35: 47–63

Boriani A, Origoni Giobbi E, Borghi A, Caironi V (1990) The evolution of the ''Serie dei Laghi'' (Strona-Ceneri and Scisti dei Laghi): the upper component of the Ivrea-Verbano crustal section; Southern Alps, North Italy and Ticino, Switzerland. Tectonophysics 182: 103–118

Boriani A, Origoni Giobbi E, Del Moro A (1982/83) Composition, level of intrusion and age of the ''Serie dei Laghi'' orthogneisses (Northern Italy-Ticino, Switzerland). Rend Soc Ital Mineral Petrol 38: 191–205

Boriani A, Villa IM (1997) Geochronology of regional metamorphism in the Ivrea Verbano Zone and Serie dei Laghi, Italian Alps. Schweiz Mineral Petrogr Mitt 77: 381–401

Bürgi A, Klötzli U (1990) New data on the evolutionary history of the Ivrea zone (northern Italy). Swiss Assoc Petrol Geol Eng Bull 56: 49–70

Caggianelli A, Del Moro A, Paglionico A, Piccarreta G, Pinarelli L, Rottura A (1991) Lower crustal granite genesis connected with chemical fractionation in the continental crust of Calabria (Southern Italy). Eur J Mineral 3: 159–180

Caironi V (1995) Zircon typology in metasediments from the Strona-Ceneri Zone (Serie dei Laghi, Western Southern Alps): indications on their protoliths and evolution. Schweiz Mineral Petrogr Mitt 75: 43–57

Cartwright I (1997) Permeability generation and resetting of tracers during metamorphic fluid flow: implications for advection-dispersion models. Contrib Mineral Petrol 12: 198–208

Compston W, Williams IS, Meyer C (1984) U–Pb geochronology of zircon from lunar breccia 73217 using a sensitive high mass-resolution ion microprobe. J Geophys Res 89B: 525–534

Condie KC (1997) Plate tectonics and crustal evolution. 3rd edn. Pergamon Press

Corfu F, Hanchar JM, Hoskin PWO, Kinny P (2003) Atlas of zircon textures. In: Hanchar JM, Hoskin PWO (eds) Zircon. Rev Mineral Geochem 53: 469–500

Cumming GL, Koeppel V, Ferrario A (1987) A lead isotope study of the northeastern Ivrea Zone and the adjoining Ceneri zone (N-Italy): evidence for a contaminated subcontinental mantle. Contrib Mineral Petrol 97: 19–30

De Waele B, Wingate MTD, Fitzsimons ICW, Mapani BSE (2003) Untying the Kibaran knot: a reassessment of Mesoproterozoic correlations in southern Africa based on SHRIMP U–Pb data from the Irumide belt. Geology 31: 509–512

Drake AA Jr (1986) Geologic map of the Fairfax quadrangle, Fairfax County, Virginia: U.S. Geological Survey Geologic Quadrangle Map GQ-1600, scale 1:24,000

Drake AA Jr (1989) Metamorphic rocks of the Potomac terrane in the Potomac Valley of Virginia and Maryland. In: International Geological Congress, 28th, Field Trip Guidebook T202. Washington, DC, American Geophysical Union, 22 pp

Fountain DM (1976) The Ivrea-Verbano and Strona-Ceneri Zones, Northern Italy: a cross section of the continental crust. New evidence from seismic velocities of rock samples. Tectonophysics 33: 145–165

Frei R, Villa IM, Nägler THF, Kramers JD, Przybylowicz WJ, Prozesky VM, Hofmann BA, Kramber BS (1997) Single mineral dating by the Pb-Pb step-leaching method: assessing the mechanisms. Geochim Cosmochim Acta 61: 393–414

Gerdes ML, Baumgartner LP, Person M (1995) Stochastic permeability models of fluid flow during contact metamorphism. Geology 23: 945–948

Giobbi Mancini E, Bergomi MA, Boriani A (2004) Petrology and age of a bimodal association (LAG – leptyno-amphibolitic group) in the basement of Southern Alps (Serie dei Laghi, N-Italy, Ticino – CH). 32nd IGC (Florence, 2004), Abstract Volume, part 2, 1060 pp

Giobbi Mancini E, Boriani A, Villa IM (2003) Pre-Alpine ophiolites in the basement of Southern Alps: the presence of a bimodal association (LAG-Leptyno-Amphibolitic group) in the Serie dei Laghi (N-Italy, Ticino-CH). Rend Fis Acc Lincei 14(s 9): 79–99

Giobbi Origoni E, Zappone A, Boriani A, Bocchio R, Morten L (1997) Relics of pre-Alpine ophiolites in the Serie dei Laghi (Western Southern Alps). Schweiz Mineral Petrogr Mitt 77: 187–207

Guy B (1993) Mathematical revision of Korzhinskii's theory of infiltration metasomatic zoning. Eur J Mineral 5: 317–339

Hanchar JM, Miller CF (1993) Zircon zonation patterns as revealed by cathodoluminescence and back-scattered electron images: implications for interpretation of complex crustal histories. Chem Geol 110: 1–13

Hanchar JM, Rudnick RL (1995) Revealing hidden structures: the application of cathodoluminescence and back-scattered electron imaging to dating zircons from lower crustal xenoliths. Lithos 36: 289–303

Harris NBW, Gravestock P, Inger S (1992) Ion microprobe determinations of trace-element concentrations in garnets from anatectic assemblages. Chem Geol 100: 41–49

Hart SR (1984) A large-scale isotope anomaly in the southern hemisphere mantle. Nature 309: 753–757

Hasalova P, Stipska P, Powell R, Schulmann K (2006) The role of melt infiltration in the formation of migmatitic orthogneiss. Geolines 20: 48–49

Henk A, Franz L, Teufel S, Oncken O (1997) Magmatic underplating, extension, and crustal reequilibration: insights from a cross section through the Ivrea Zone and Strona-Ceneri Zone, northern Italy. J Geol 105: 367–377

Hofmann AW (1972) Chromatographic theory of infiltration metasomatism and its application to feldspars. Amer J Sci 272: 60–90

Kano T (1991) Metasomatic origin of augen gneisses and related mylonitic rocks in the Hida metamorphic complex, central Japan. Mineral Petrol 45: 29–45

Kleinhanns IC, Kreissig K, Kamber BS, Meisel TH, Naegler THF, Kramers JD (2002) Combined chemical separation of Lu, Hf, Sm, Nd, and REEs from a single rock digest: precise and accurate isotope determinations of Lu-Hf and Sm-Nd using multi-collector ICPMS. Analyt Chem 74: 67–73

Köppel V, Grünenfelder M (1971) A study of inherited and newly formed zircons from metaarenites and granitised sediments of the Strona-Ceneri Zone (Southern Alps). Schweiz Mineral Petrogr Mitt 52: 385–410

Kretz R (1983) Symbols of rock forming minerals. Am Mineral 68: 277–279

Kröner A, O'Brien PJ, Nemchin AA, Pidgeon RT (2000) Zircon ages for high pressure granulites from South Bohemia, Czech Republic, and their connection to Carboniferous high temperature processes. Contrib Mineral Petrol 138: 127–142

Ludwig KR (2001a) User's Manual for Isoplot/Ex rev. 2.49: a geochronological toolkit for Microsoft Excel. Berkeley Geochronology Center Spec Publ 1a: 59 pp

Ludwig KR (2001b) SQUID 1.02, A User's Manual. Berkeley Geochronology Center Sp Pub 2

Manning CE, Ingebritsen SE (1999) Permeability of the continental crust: implications of geothermal data and metamorphic systems. Rev Geophy 37: 127–150

McCaig AM, Knipe J (1990) Mass-transport mechanisms in deforming rocks: recognition using microstructural and microchemical criteria. Geology 18: 824–827

Milord I, Sawyer EW (2003) Schlieren formation in diatexite migmatite: examples from the St. Malo migmatite terrane, France. J Metam Geol 21: 347–362

Milord I, Sawyer EW, Brown M (2001) Formation of diatexite migmatite and granite magma during anatexis of semi-pelitic metasedimentary rocks: an example from St. Malo, France. J Petrol 42: 487–505

Montel JM, Vielzeuf D (1997) Partial melting of metagreywackes, Part II. Compositions of minerals and melts. Contrib Mineral Petrol 128: 176–196

Nakamura M, Watson EB (2001) Experimental study of acqueous fluid infiltration into quartzite: implications for the kinetics of fluid redistribution and grain growth driven by interfacial energy reduction. Geofluids 1: 73–89

Nelson DR (1997) Compilation of SHRIMP U–Pb zircon geochronology data. Geol Survey West. Australia Record 1997/2: 189 pp

Otamendi JE, Patino Douce AE (2001) Partial melting of aluminous metagreywackes in the northern Sierra de Comechingones, Central Argentina. J Petrol 42: 1751–1772

Pettke T, Diamond LW (1995) Rb-Sr isotopic analysis of fluid inclusions in quartz; evaluation of bulk extraction procedures and geochronometer systematics using synthetic fluid inclusions. Geochim Cosmochim Acta 59: 4009–4027

Pezzotta F, Pinarelli L (1994) The magmatic evolution of Ordovician metagranitoids of the Serie dei Laghi (Southern Alps): inferences from petrological, geochemical, and Sr and Nd isotope data. Per Mineral 63: 127–147

Pidgeon RT, Macabira MJB, Lafon JM (2000) Th-U-Pb isotopic system and internal structures of complex zircon from an enderbite from the Pium Complex, Carajas Province, Brazil: evidence for the ages of granulite facies metamorphism and the protolith of the enderbite. Chem Geol 166: 159–171

Pin C (1990) Evolution of the lower crust in the Ivrea zone: a model based on isotopic and geochemical data. In: Vielzeuf D, Vidal PH (eds) Granulites and crustal evolution. Kluwer Academic Publishers, The Netherlands, pp 87–110

Pinarelli L, Boriani A (2007) Tracing metamorphism, magmatism and tectonics in the southern Alps (Italy): constraints from Rb-Sr and Pb-Pb geochronology, and isotope geochemistry. Per Mineral 76: 5–24

Quick JE, Sinigoi S, Mayer A (1994) Emplacement dynamics of large mafic intrusions in the lower crust, Ivrea-Verbano Zone, northern Italy. J Geophys Res 99 (B11): 21559–21573

Reinhard M (1964) Ueber das Grundgebirge des Sottoceneri in Sued-Tessin und die darin auftretenden Ganggesteine. Beitr Geol Karte Schweiz, NF 117: 89 pp

Sawyer EW (1986) The role of partial melting and fractional crystallization in determining discordant migmatite leucosome compositions. J Petrol 28: 445–473

Schoenberg R, Naegler THF, Kramers JD (2000) Precise Os isotope ratio and Re-Os isotope dilution measurements down to the picogram level using multicollector inductively coupled plasma mass spectrometry. Int J Mass Spec 197: 85–94

Sibson RH (1996) Structural permeability of fluid-driven fault-fracture meshes. J Struct Geol 18: 1031–1042

Sun S, McDonough WF (1989) Chemical and isotopic systematics of oceanic basalts: implications for mantle composition and processes. In: Saunders AD, Norry MG (eds) Magmatism in the ocean basins. Geol Soc Amer Spec Publ 42: 313–345

Taylor SR, McLennan SM (1985) The continental crust: its composition and evolution. Blackwell, London

Vassallo JJ, Vernon RH (2000) Origin of megacrystic felsic gneisses at Broken Hill. Austral J Earth Sci 47: 733–748

Vavra G, Gebauer D, Schmid R, Compston W (1996) Multiple zircon growth and recrystallization during polyphase Late Carboniferous to Triassic metamorphism in granulites of the Ivrea Zone (southern Alps) – an ion microprobe (SHRIMP) study. Contrib Mineral Petrol 122: 337–359

Vernon RH, Paterson SR (2002) Igneous origin of K-feldspar megacrysts in deformed granite of the Papoose Flat Pluton, California, USA. Electron Geosci 7: 31–39

Vielzeuf D, Montel JM (1994) Partial melting of metagreywackes. Part I. Fluid-absent experiments and phase relationships. Contrib Mineral Petrol 117: 375–393

Voshage H, Hofmann AW, Mazzucchelli M, Rivalenti G, Sinigoi S, Raczek I, Demarchi G (1990) Isotopic evidence from the Ivrea Zone for a hybrid lower crust formed by magmatic underplating. Nature 347: 731–736

Voshage H, Hunziker JC, Hofmann AW, Zingg A (1987) A Nd and Sr isotopic study of the Ivrea zone, Southern Alps, N-Italy. Contrib Mineral Petrol 97: 31–42

Watson B (1982) Melt infiltration and magma evolution. Geology 10: 236–240

Watt GR, Harley SL (1993) Accessory phase controls on the geochemistry of crustal melts and restites produced during water-undersaturated partial melting. Contrib Mineral Petrol 114: 550–566

Weinberg RF, Searle MP (1999) Volatile-assisted intrusion and autometasomatism of leucogranites in the Khumbu Himalaya, Nepal. J Geol 107: 27–48

Wohlers A, Baumgartner L (2004) Melt infiltration textures in migmatites of the Little Cottonwood contact aureole, Utah, USA. Geol Soc Amer 36–5: 202

Zartman RE, Doe BR (1981) Plumbotectonics – the model. Tectonophysics 75: 135–162

Zurbriggen R, Franz L, Handy MR (1997) Pre-Variscan deformation, metamorphism and magmatism in the Strona-Ceneri Zone (southern Alps of northern Italy and southern Switzerland). Schweiz Mineral Petrogr Mitt 77: 361–380